Skin and Subcutaneous Tissue

2

Maura Valle and Maria Pia Zamorani

CONTENTS

2.1 Histologic Considerations

From the histologic point of view, the skin varies in thickness from 1.5 to 4.0 mm and is composed of a superficial layer and a deep layer – the epidermis and the dermis, respectively (Fig. 2.1a). The epidermis is made of stratified epithelium, and can be divided into two main layers: the superficial stratum corneum, which is made of closely packed flattened dead cells, and the deep germinative zone (consisting of the stratum basale, stratum spinosum and stratum granulosum). In regions that are not subject to pressure, the epidermis is thin and hairy, whereas in areas undergoing attrition and local shocks (i.e., palms of the hands and soles of the feet), the skin is hairless and may thicken to an even greater extent as a result of a hypertrophied stratum corneum. Deep to the epidermis, the dermis is a thick layer containing large amounts of collagen and a rich network of vessels, lymphatics and nerve endings. It can be divided into a deep reticular layer, which is composed of bulky connective tissue, and a superficial papillary layer, which interdigitates with the base of the epidermis and provides an important mechanical and metabolic support to the overlying epidermis. Additional structures housed within the dermis are sebaceous and sweat glands, hair follicles and erector pili muscles.

Deep to the dermis, the subcutaneous tissue lies between the skin and the fascia (Fig. 2.1a). It acts as a gliding plane between these structures, thus protecting deeper areas from acute and chronic trauma; it also stores fat and participates in temperature control. The subcutaneous tissue is formed by a network of connective tissue septa and fat lobules. The overall size and extent of these septa vary at different sites of the body: they may be tiny in "loose" skin or compact when the skin is firmly attached to the underlying fascia. In normal conditions, the thickness of the subcutaneous tissue varies greatly depending on the amount of fat contained within. In some areas of the body, such as the dorsal aspect of the hand, the fat is sparse, while in other regions, such as the thighs and the buttocks, it is abundant. The amount and distribution of subcutaneous fat is also related to the individual body habitus, sex and the meteorologic environment. Discrete vessels, lymphatics, sensory nerve endings and hair follicles are contained in the subcutaneous tissue.

In areas where moving structures are tightly apposed, superficial "attritional" bursae separate the skin from the underlying tissues, and especially from the bone. These bursae are synovial-lined sacs tethered by dermis and periosteum. In the fingers and toes, the nails include the nail plate, the nail folds, the epidermis, the germinative matrix and the

M. Valle, MD
Staff Radiologist, Reparto di Radiologia, Istituto Scientifico "Giannina Gaslini", Largo Gaslini 5, 16148 Genova, Italy
M. P. Zamorani, MD
Unité de Recherche et Dévelopement, Clinique des Grangettes, 7, ch. des Grangettes, 1224 Genève, Switzerland

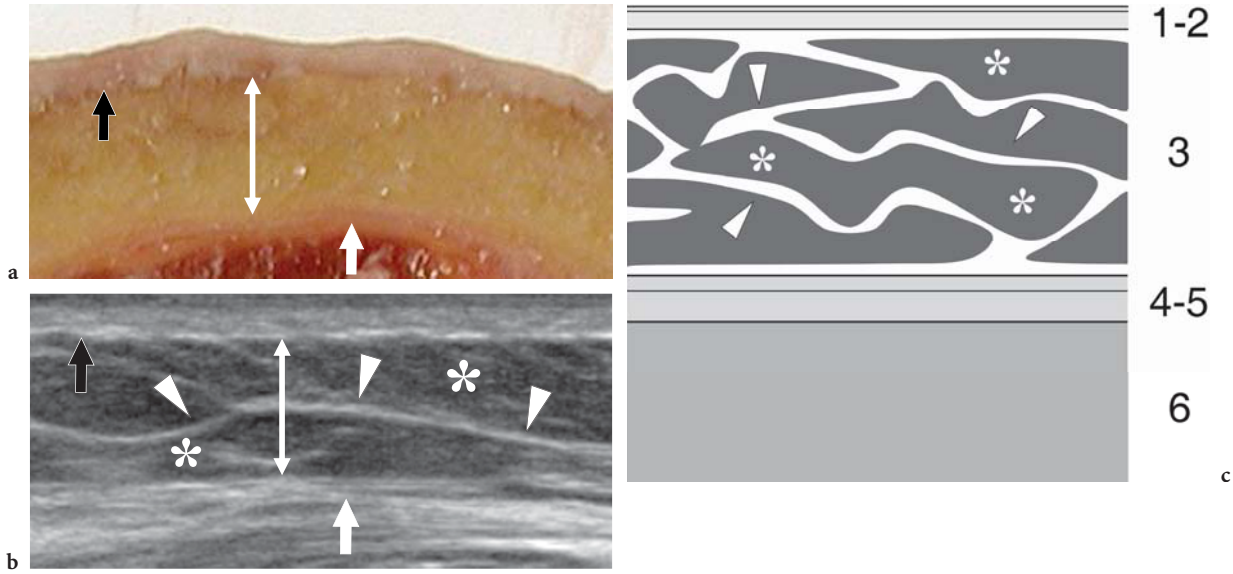

Fig. 2.1a–c. Normal skin and subcutaneous tissue. **a** Photograph of a cadaveric cross-section of the anterior thigh demonstrates a superficial layer reflecting the epidermis and dermis (*black arrow*), an intermediate thick layer representing fat contained in the subcutaneous tissue (*double arrow*) and a deep thin layer, located just superficial to the quadriceps muscle, due to the juxtaposed superficial and deep fascia (*white arrow*). **b** Corresponding transverse 17–5 MHz US image obtained in a healthy subject demonstrates the three tissue layers shown in **a**: the epidermis and dermis (*black arrow*) are homogeneously hyperechoic; the subcutaneous tissue (*double arrow*) includes a hypoechoic background reflecting fat lobules (*asterisks*) and hyperechoic strands (*arrowheads*) due to connective septa; the apposed superficial and quadriceps fasciae appear hyperechoic (*white arrow*). **c** Schematic drawing shows the normal architecture of the superficial tissues. From surface downward, note the epidermis and dermis (*1*, *2*); the subcutaneous tissue (*3*) containing fat lobules (*asterisks*) separated by connective tissue strands (*arrowheads*); the superficial and deep (muscle) fascia (*4-5*); and the muscles (*6*)

dermis. The nail plate is similar to the stratum corneum of the skin. The proximal nail plate and the lateral folds overlie its sides. The undersurface of the nail plate is lined by squamous epithelium, which is continuous with that of the proximal nail fold and thickens at the nail root to form the germinative matrix.

2.2 Normal US Findings

US of the skin is almost exclusively performed by dermatologists, who make use of dedicated equipment with ultra-high-frequency transducers working at 20–100 MHz. Although the in-plane resolution of these transducer is as high as <50 µm, the depth of field is markedly limited at such high frequencies, and is reported to be 1 mm or less (Erickson 1997). Therefore, these transducers are not suitable for a combined evaluation of the subcutaneous tissue in its full thickness. At 20 MHz, the echogenic dermis can be distinguished from the hypoechoic subcutaneous fat and pilosebaceous units are recognizable (Fornage et al. 1993). The thick epidermis of the palm and sole can be recognized as well. In sites covered by thin hairy skin, the epidermis can be appreciated as an individual structure by means of 40 MHz frequency transducers. In aged skin, a subepidermal low-echogenic band is often appreciated as a result of increased water content. Normal skin thickness ranges have been established with US at different body sites (Fornage and Deshayes, 1986; Fornage et al. 1993). Further details on the US examination of the skin are beyond the scope of this chapter.

An adequate assessment of the subcutaneous tissue can be efficiently performed be means of "less specialized" high-resolution transducers characterized by the same frequency range (5–15 MHz) appropriate for other musculoskeletal examinations. The type and frequency of the selected transducer vary depending on the region of the body to be examined. For the thin subcutaneous tissue of the dorsum of the hand and wrist, linear-array transducers working at a center frequency >7.5–10 MHz are the most appropriate. Superficial focusing capabilities and a thin

stand-off pad are additional requirements. On the other hand, if the thick subcutaneous fat of the lateral part of the proximal thigh is the target of examination, US should be performed at lower frequencies, even as low as 5 MHz if needed, to obtain sufficient penetration for a reliable assessment. A large amount of gel that produces a homogeneous, uniform contact between probe and skin may be required to avoid formation of small air bubbles. Examination of certain body areas, such as the plantar aspect of the calcaneus, can be difficult to perform because the thickened stratum corneum can cause considerable US beam attenuation, leading to a decreased signal-to-noise ratio of the US image. The subcutaneous tissue appears at US as a discrete hypoechoic layer characterized by a hypoechoic background of fat and hyperechoic linear echoes corresponding to a web of connective septa (Fig. 2.1b). These septa run, for the most part, parallel or slightly obliquely to the skin surface. Subcutaneous veins are displayed as elongated or rounded echo-free structures that run inside the larger septa. Owing to their low blood pressure, normal veins collapse if pressure is applied over them with the probe. In selected cases, color Doppler imaging can be used to demonstrate blood flow signals within the vessels. Small sensory nerves can be appreciated as very tiny fascicular structures coursing alongside the largest superficial veins (Fig. 2.2). Both veins and sensitive nerves usually run in the deep part of the subcutaneous tissue. Knowledge of the close relationship of nerves with adjacent veins makes their detection easier: the sural nerve, for instance, can be easily detected at the posterior distal leg because it is satellite to the adjacent small saphenous vein. Lymphatics housed within the connective septa cannot be visualized with US, unless distended by fluid as in the case of subcutaneous edema. Dynamic US examination while applying either different degrees of pressure with the probe or finger palpation or manual mobilization of the skin is essential for evaluating masses, fluid collections and fibrosis of the subcutaneous tissue.

2.3 Pathologic Findings

2.3.1 Skin Abnormalities

A detailed description of the US findings observed in the wide range of pathologic conditions affecting the skin is beyond the scope of this chapter. Briefly, the use of specialized 20–50 MHz transducers has been mainly proposed in the following settings: measurement of the thickness and depth of skin tumors prior to cryosurgery, laser surgery or radiotherapy; and monitoring the effects of therapy in chronic inflammatory processes, such as psoriasis (Schmid-Wendtner and Burgdorf 2005).

Skin tumors appear as focal hypoechoic nodules, clearly distinguishable from the surrounding normal dermis because of the higher echogenicity of the latter. In most cases, including melanomas, the lateral boundaries of the tumor are ill defined, whereas there is a clear-cut basal demarcation. It has been reported that in the assessment of melanoma thickness the accuracy of US is comparable to that of histology. In tumor staging, the main limitations of US are related to overestimation of the tumor size due to either surrounding inflammatory infiltration

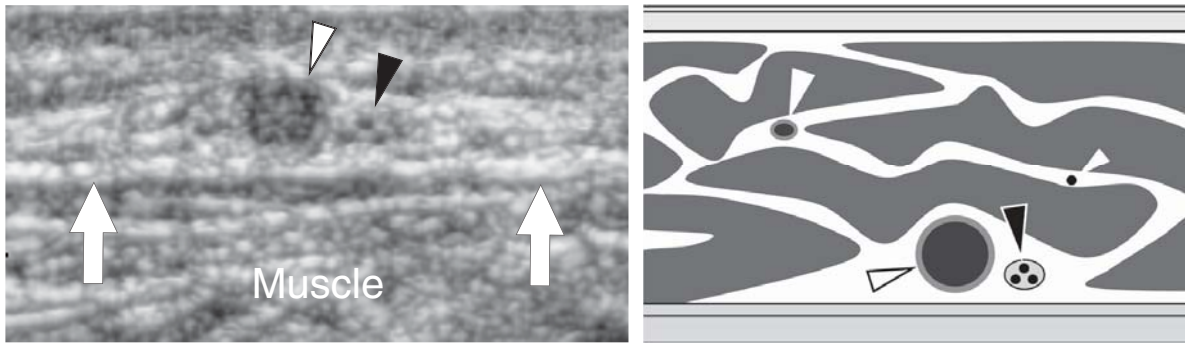

a b

Fig. 2.2a,b. Subcutaneous veins and nerves. **a** Transverse 12–5 MHz US image obtained over the posterior calf demonstrates the small saphenous vein (*white arrowhead*) and the adjacent sural nerve (*black arrowhead*) running in the deep subcutaneous tissue. Detection of the larger vein is a useful landmark for recognition of the smaller nerve. *Arrows* indicate the fascial plane. **b** Schematic drawing correlation shows subcutaneous veins (*white arrowheads*) and the nerve (*black arrowhead*) coursing in the connective spaces which separate fat lobules

which, being hypoechoic, cannot be discriminated from neoplastic tissue, or inclusion of other structures (i.e., hair follicles and sweat glands) as part of the lesion itself. These errors are less frequent in the evaluation of advanced-stage tumors, when peritumoral inflammatory infiltration is generally less conspicuous (Fig. 2.3a). In addition, a precise demarcation of the tumor from the subcutaneous fat is often unfeasible in tumors extending deep to the dermis-subcutaneous separation plane due to their similar hypoechoic echotextures. Overall, the diagnostic value of US for staging skin tumors has been significantly downgraded in recent years and relegated to restricted use in a few specialized dermatologic centers. In contrast, in the postoperative follow-up of patients with melanoma, US has proved helpful in guiding the management strategy of the referring physician by facilitating detection of nonpalpable metastases occurring in the area of the original scar or skin graft or along the pathway of lymphatic drainage. In addition, US may add as well as in differentiating benign from malignant palpable masses by guiding definitive biopsy, and in the assessment of pharmacodynamic response to chemotherapy (Nazarian et al. 1996).

Among non-neoplastic conditions, cutaneous scars appear as ill-defined focal hypoechoic bands with posterior acoustic shadowing usually extending into the subcutaneous tissue with a definite straight course (Fig. 2.3b). The examiner should be aware of the appearance of superficial scars because they may indicate the site and path of previous surgery or penetrating wounds. In scleroderma, the measurement of skin thickness by high-resolution US in clinically involved and non-involved areas can support an early diagnosis. In this setting, US may allow detection of the different stages of disease (Akesson et al. 1986; Scheja and Akesson 1997; Brocks et al. 2000; Clements et al. 2000).

2.3.2 Subcutaneous Tissue Abnormalities

2.3.2.1 Edema

US demonstrates subcutaneous edema as a hyperechoic appearance of fat lobules. In the early stages, oedematous changes tend to involve the deep layer of the subcutaneous tissue, which becomes hypoanechoic due to fluid accumulation related to dilation of lymphatics, whereas the most superficial layers of the subcutaneous tissue retain a normal appearance (Fig. 2.4a,b). With progressive accumulation of fluid, the connective septa enlarge and become anechoic strands as a result of distension of the superficial network of lymphatic channels, until the fat lobules become individualized structures separated from one another by anechoic fluid (Fig. 2.4c-e). One should realize that the fluid that surrounds the lobules is not free but contained within dilated lymphatic

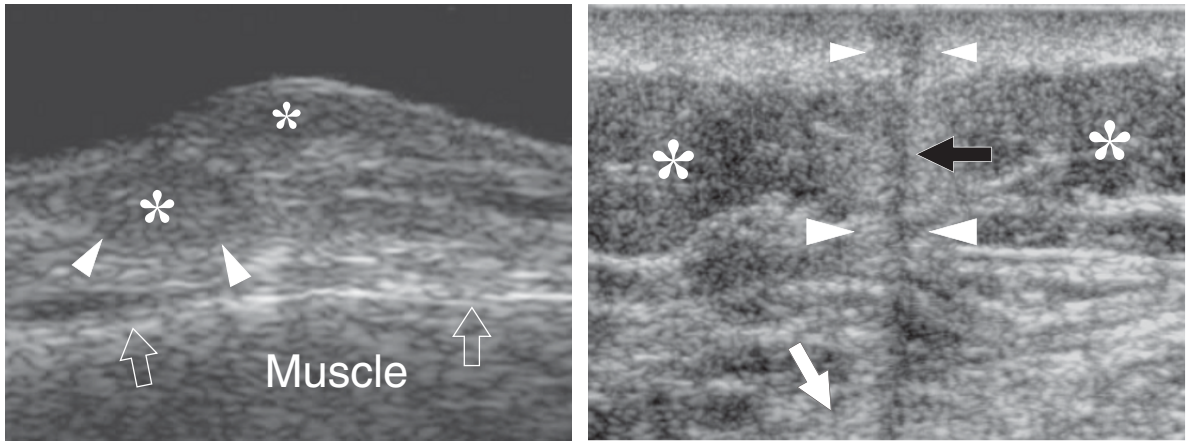

Fig. 2.3a,b. Skin abnormalities. **a** Mycosis fungoides/Sézary syndrome. A 15-10-MHz US image over a skin papula in the anterior abdominal wall demonstrates a superficial ill-defined hypoechoic tumor (*asterisks*) with signs of infiltration of the subcutaneous fat (*arrowheads*). *Arrows*, fascial plane. **b** Postoperative scar. Transverse 12–5 MHz US image over the lateral thigh in a patient who underwent previous resection for a liposarcoma shows a hypoechoic straight band (*black arrow*) extending with a vertical course from the skin downward, reflecting a postoperative scar. Note that the hypoechoic band is surrounded by a peripheral hyperechoic halo (*arrowheads*) reflecting fibrotic changes in the adjacent subcutaneous (*asterisks*) and underlying muscle (*white arrow*)

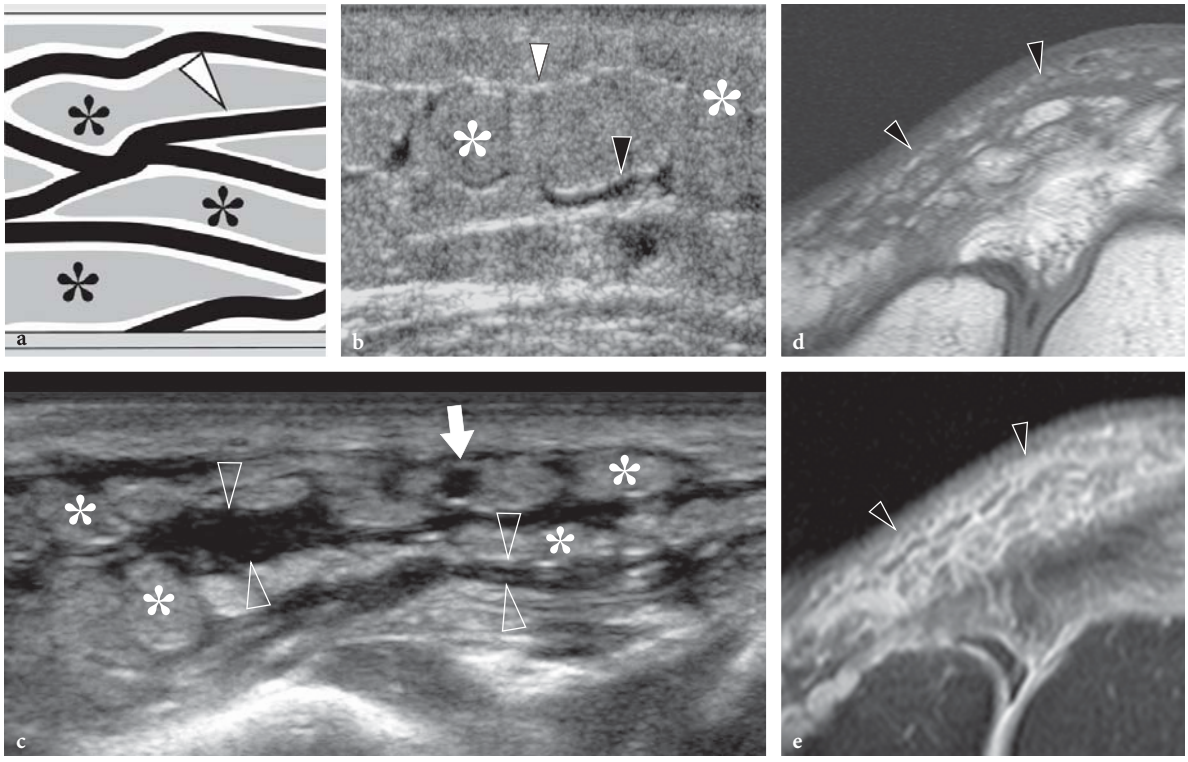

Fig. 2.4a–e. Subcutaneous tissue edema. **a** Schematic drawing illustrates the arrangement of fluid-filled dilated lymphatic channels (*in black*) within the subcutaneous tissue in cases of noninflammatory edema. Lymphatic vessels travel in the hyperechoic connective tissue septa (*arrowhead*) among fat lobules (*asterisks*). Once these vessels are distended, they make these septa thickened and hypoechoic. **b** Mild subcutaneous edema. Transverse 12-5-MHz US image over the pretibial region shows an increased echogenicity of fat lobules (*asterisks*) and fluid distention of the lymphatics running in the deep connective septa (*black arrowhead*). Note the normal appearance of the more superficial connective septa (*white arrowhead*). **c** Transverse 17-5-MHz US extended-field-of-view image of the anteromedial knee with correlative **d** T1-weighted and **e** T2-weighted MR images in a patient with severe local subcutaneous tissue edema demonstrates striking enlargement and fluid distension of all septa (*open arrowheads*) of the subcutaneous tissue, reflecting overt dilation of lymphatic channels. Note the fat lobules (*asterisks*), which appear as individual structures separated by the intervening fluid. *Arrow* indicates a patent superficial vein

channels. These findings are typically encountered in deep venous thrombosis or in local fluid collections. Graded pressure applied with the probe does not cause collapse of the anechoic strands. In selected cases, Doppler imaging can differentiate edema within the lymphatics from the adjacent enlarged subcutaneous veins.

2.3.2.2 Cellulitis, Abscess and Necrotizing Fasciitis

Subcutaneous infections, which are referred to as cellulitis or panniculitis, are commonly encountered in clinical practice and properly assessed at physical examination. In most instances, the causative agents of cellulitis are group A *Streptococcus pyogenes* or *Staphylococcus aureus*. In these cases, US may have an important diagnostic value, especially for differentiating cellulitis from an abscess and distinguishing the latter from other soft-tissue masses (Chau and Griffith 2005). US can stage local spread of infection to deep tissue layers (involvement of muscles, bursae, tendon sheaths and joints), and can identify possible causative factors (e.g., foreign bodies, retained gauzes). In addition, it provides accurate guidance for diagnostic or therapeutic aspiration procedures (Chau and Griffith 2005). In cellulitis, US demonstrates an irregular ill-defined hyperechoic appearance of fat with blurring of tissue planes, progressing to hypoechoic strands reflecting edema (Nessi et al. 1990; Robben 2004). This appearance is nonspecific and cannot be distinguished from noninfectious causes of soft-tissue edema on the basis of echotextural findings alone (Struk et al. 2001; Robben 2004).

Color and power Doppler imaging may help the clinical diagnosis by depicting a hypervascular pattern in cellulitis (Cardinal et al. 2001) (Fig. 2.5a,b). Phlebitis and occlusion of superficial veins may also be observed as associated findings. If untreated, infectious cellulitis can progress to abscess formation (Fig. 2.5c,d).

In most cases, a subcutaneous abscess is demonstrated as an irregular fluid-filled hypoechoic area with posterior acoustic enhancement, containing variable amount of echogenic debris (pus) (Fig. 2.5c,d). Fluid-fluid levels within the collection with dependent layering of the more echogenic particulate material can be noted. In highly echogenic collections, a slight pressure with the probe or the fingers may help to confirm the liquid nature of the mass by causing fluctuation of the particles (Loyer et al. 1996). Doppler imaging modalities typically show hyperemic blood flow within the abscess wall and the surrounding tissues (Arslan et al. 1998). Cellulitis being essentially a clinical diagnosis, the main diagnostic role of US is to rule out deep venous thrombosis and

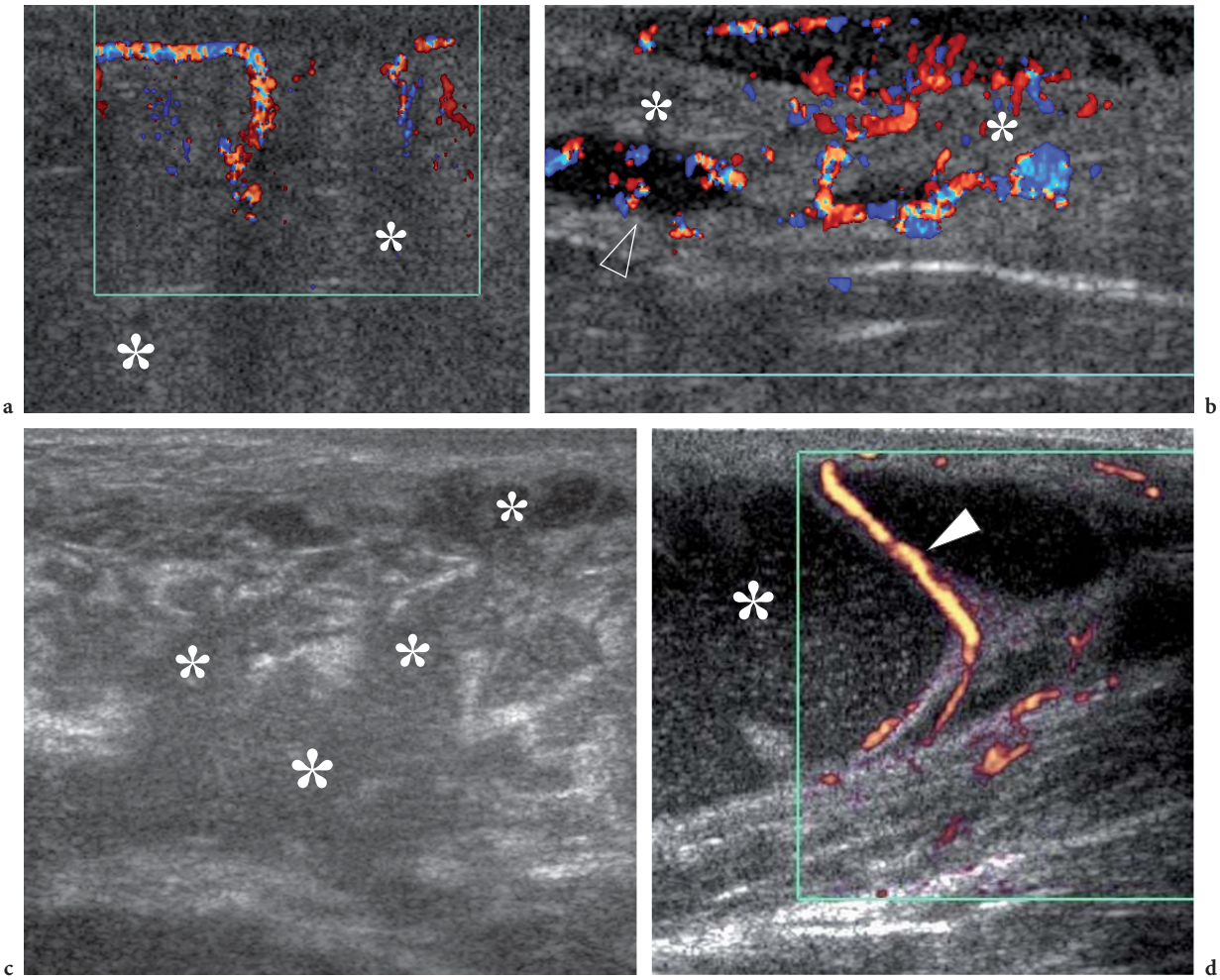

Fig. 2.5a–d. Subcutaneous tissue infection. **a,b** Cellulitis and **c,d** abscess. Images are from different patients. **a** Color Doppler 12–5 MHz US image reveals a diffusely increased echogenicity of the subcutaneous fat (*asterisks*) with blurring of the definition of connective septa and fatty lobules, and an increased vasculature. **b** Color Doppler 12–5 MHz US image shows signs of initial progression of cellulitis into abscess. There is diffuse subcutaneous edema with hyperechoic fatty lobules (*asterisks*) alternating with irregular hypoechoic areas (*arrowhead*) filled with Doppler signals. An intense hypervascular pattern is seen. **c** Gray-scale 12–5 MHz US image over the gluteal region in patient with tuberculosis demonstrates coalescence of hypoechoic serpiginous areas into a large hypoechoic abscess (*asterisk*) with loss of Doppler signals. **d** Power Doppler 12–5 MHz US image of a forearm abscess in an HIV-positive patient shows a large cavity filled with echogenic particulate material (*asterisk*) inside the subcutaneous tissue, displacing the fat lobules. Fluctuation of the echogenic material filling the abscess could be obtained on compression. The abscess dislocates and stretches the connective septa and the small vessels (*arrowheads*) contained within them.

to identify an underlying abscess. Even if an abscess is not found but infection-related symptoms persist, US examination should be repeated because liquefaction may manifest with time (Robben 2004). In addition, if the abscess lies in proximity to the bone, US may reveal the osseous origin of the infection by depicting hypoechoic subperiosteal fluid (Robben 2004).

Often associated with a previous trauma (e.g., open wound, insect bite), necrotizing fasciitis is a rare, rapidly progressive, life-threatening infection involving the subcutaneous tissue, fascia and surrounding soft-tissue structures, including muscles. A variety of aerobic and anaerobic bacteria may be involved as causative agents of necrotizing fasciitis, group A *Streptococcus* being the most common. In most cases, the patient is diabetic, immunocompromised or severely ill with profound toxicity. Although US is not rewarding at the early stages of infection when soft-tissue abnormalities may mimic cellulitis, it may be helpful for demonstrating the extent of fascial thickening and accumulation of cloudy fluid along the deep fascial layer (Fig. 2.6a). An amount of fluid >4 mm in depth has been regarded as highly sensitive and specific for the diagnosis of necrotizing fasciitis (Yen et al. 2002). In addition, US can reveal loculated abscesses in the fascial plane – allowing US-guided diagnostic aspiration – and gas formation in soft tissues in advanced disease (Robben 2004; Wilson 2004). Gas gangrene, which is produced by organisms of bowel origin or by *Clostridium*, is an ominous sign (Fig. 2.6b). Aggressive surgical debridement and a course of broad-spectrum antibiotics are critical for the patient's survival.

2.3.2.3 Fatty Atrophy

Focal reabsorption of the subcutaneous tissue and depigmentation of the overlying skin can be observed following local inadvertent injection of long-acting corticosteroids (Canturk et al. 2004). This "side-effect" is somewhat related to the catabolic effect of the drug: thinning of the subcutaneous fat is dose-related, may be appreciated up to complete reabsorption of the fatty tissue layer and shows a maximal decrease 4–8 weeks after a single injection of steroids (Gomez et al. 1982). US is a reliable means to confirm the presence of focal shrinkage of the subcutaneous fat by comparing the affected side with either the contralateral healthy side or an adjacent normal area. In clinical practice, focal areas of subcutaneous atrophy may occur around the radial head following steroid injection for treatment of tennis elbow and at the buttock secondary to intramuscular injections. Although the US appearance of subcutaneous atrophy is rather specific, awareness of the clinical history is essential to correlate the US findings with a specific causative factor.

2.3.2.4 Traumatic Injuries

In a traumatic setting, and especially in contusion traumas, changes of the subcutaneous tissue are commonly encountered. Depending on the strength and duration of the insult and the patient's state

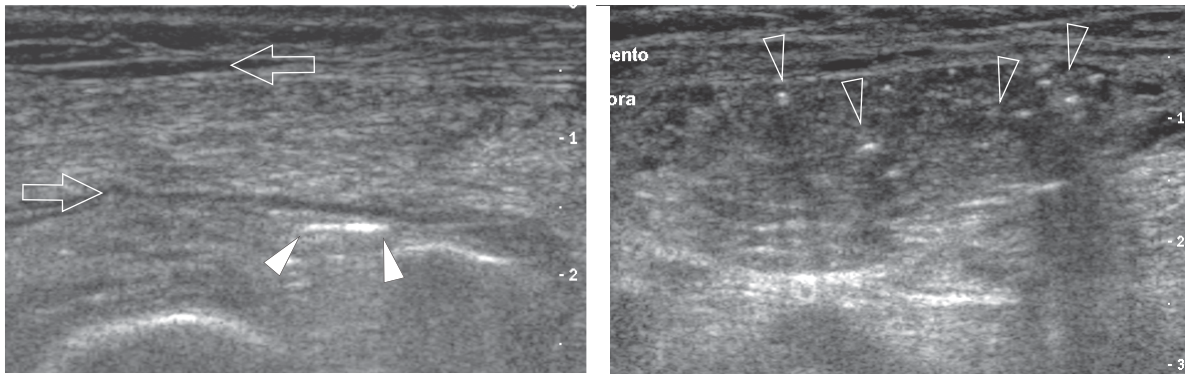

a b

Fig. 2.6a,b. Necrotizing fasciitis. Transverse 12–5 MHz US images over the lower anterolateral leg in a severely compromised diabetic patient with necrotizing fasciitis demonstrate accumulation of fluid along fascial planes (*arrows*) and scattered bright foci in the soft-tissues reflecting initial gas formation (*arrowheads*)

(anticoagulation therapy, steroids, etc.), soft-tissue abnormalities may range from simple hemorrhagic infiltration of fat lobules, to fat necrosis, hematomas and abscesses. US reveals bloody fat infiltration as an increased echogenicity of fatty lobules that can make the separation from the hyperechoic skin and the connective tissue strands of the subcutaneous tissue undefined (Fig. 2.7a). Hemorrhagic fat infiltration can be readily distinguished from simple edema because of the absence of anechoic fluid distending the connective septa. The differential diagnosis with a superficial hyperechoic lipoma is based on the clinical history and the oval, well-circumscribed appearance of the soft-tissue mass. Following a contusion trauma, subcutaneous fat necrosis may arise with edema, hemorrhage and fibrosis with lack of a discrete soft-tissue mass and volume loss of the subcutaneous tissue (Tsai et al. 1997; Ehara 1998). Fat necrosis appears as a hyperechoic focus containing hypoechoic spaces related to infarcted fat (Fernando et al. 2003) (Fig. 2.7b). In hematomas, the US appearance of the bloody collection varies over time. Soon after the blood leakage, fresh fluid may appear highly reflective up to a pseudosolid appearance because of fibrin and erythrocytes forming multiple acoustic interfaces. With time, the hematoma tends to become completely anechoic as a result of liquefaction of the clot and increases in size (Fig. 2.8a). A network of thin strands may often be seen resulting from fibrin organization (Fig. 2.8b). Fluid levels reflecting separation between serum (anechoic) and cellular components (echogenic) of blood can also be observed. Over a period of months, the hematoma eventually resolves, but a residual fibrous scar and focal retraction of the overlying skin may persist (Fig. 2.8c). As described in Chapter 12, a hematoma that has a peculiar disposition related to the subcutaneous tissue is the Morel-Lavallée lesion. This condition indicates a post-traumatic seroma which derives from local trauma usually located over the lateral aspect of the proximal thigh. The collection typically intervenes between the deep layer of the subcutaneous tissue and the fascia as a result of a shear strain mechanism causing disruption of the rich vascular plexus that pierces the fascia lata (Morel-Lavallée 1863). US depicts a Morel-Lavallée lesion as an elongated fluid collection overlying the straight echogenic appearance of the fascia (Parra et al. 1997; Mellado et al. 2004). In cases of an abscess secondary to trauma, the examiner should attempt to recognize any possible foreign body within it as the causative factor (Fig. 2.9). This is valid even if the patient denies previous open wounds, because the presence of foreign bodies requires surgical removal. In an effort to exclude a more extensive spread of infection that may deserve different treatment, the examiner should check the status of underlying regional muscles, tendon sheaths and joint spaces. Finally, a contusion trauma on the skin by a pointed, sharp object can be transmitted to the subcutaneous tissue causing laceration and focal discontinuity of fat lobules. This category of lesions results in "fat fractures"

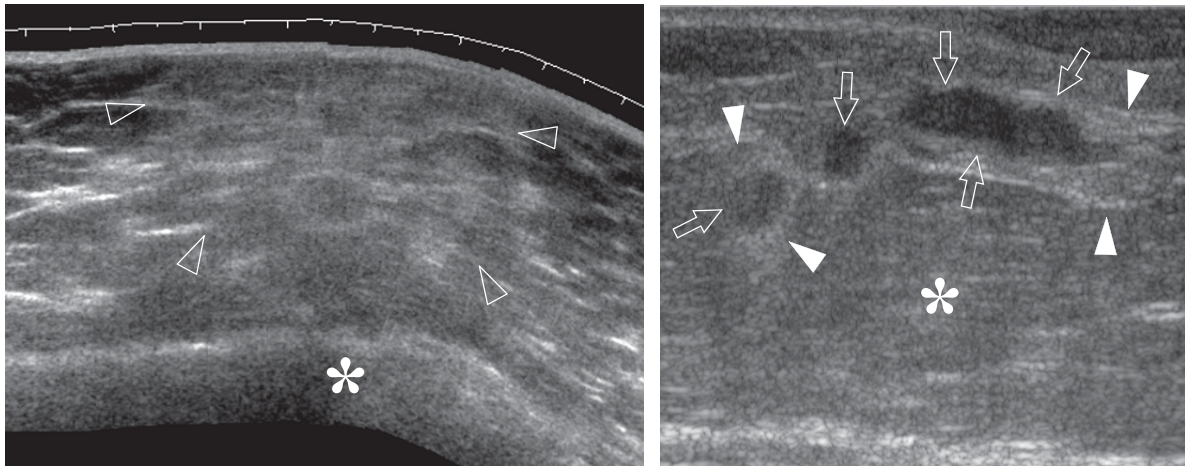

a b

Fig. 2.7a,b. Subcutaneous tissue contusion trauma and fat necrosis. **a** Transverse extended-field-of-view 12–5 MHz US image of the trochanteric region in a patient with local contusion trauma after a fall demonstrates an undefined increased echogenicity of fatty lobules (*arrowheads*) reflecting hemorrhagic fat infiltration. Note that the abnormal area is located just superficial to the osseous prominence of the greater trochanter (*asterisk*). **b** Longitudinal 12–5 MHz US image over the anterolateral thigh in another patient with previous local contusion caused by a sharp object. US shows three well-circumscribed hypoechoic areas (*arrows*) surrounded by ill-defined hyperechoic halo (*arrowheads*) within the subcutaneous tissue (*asterisk*) representing fat necrosis

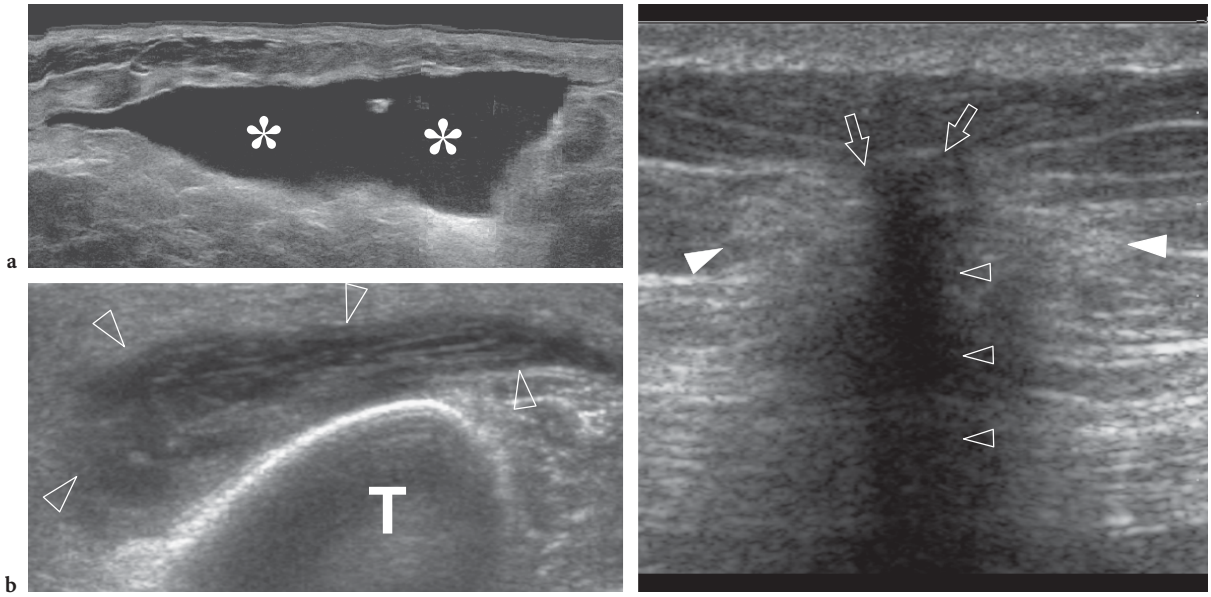

Fig. 2.8a–c. Superficial hematoma: spectrum of 12–5 MHz US appearances. **a** Hematoma of the subcutaneous tissue examined a few days after blunt trauma. US demonstrates an echo-free fluid collection (*asterisks*) reflecting the phase of clot liquefaction. **b** Pretibial hematoma (*arrowheads*) examined 15 days after trauma reveals closely packed fibrous stranding within the collection reflecting fibrin organization. *T*, tibia. **c** Residual fibrous scar following a large hematoma in the buttock. US shows the scar as a hyperechoic reflection (*arrows*) with posterior acoustic shadowing (*open arrowheads*) causing distorsion of the adjacent subcutaneous fat (*white arrowheads*)

that may mimic a tendon gap at physical examination. US can determine whether the discontinuity is limited to the subcutaneous fat or involves the deeper structures too (Thomas et al. 2001) (Fig. 2.10). Subcutaneous scars are easily depicted with US as vertically -oriented thin linear stripes surrounded by hyperechoic halo that interrupt the normal tissue layers. The abnormal tissue can extend deeply across the fascia into the muscles or the ligaments. Scars may eventually calcify (see Fig. 2.8c).

2.3.2.5 Foreign Bodies

Foreign bodies can be found in the subcutaneous tissues as the result of traumatic injuries or therapeutic procedures. In a post-traumatic setting, foreign bodies derive from open or penetrating wounds. Most are composed of plant fragments (wood splinters, thorns, etc.), metal or glass. In terms of prevalence, wood fragments are the most frequently found, fol-

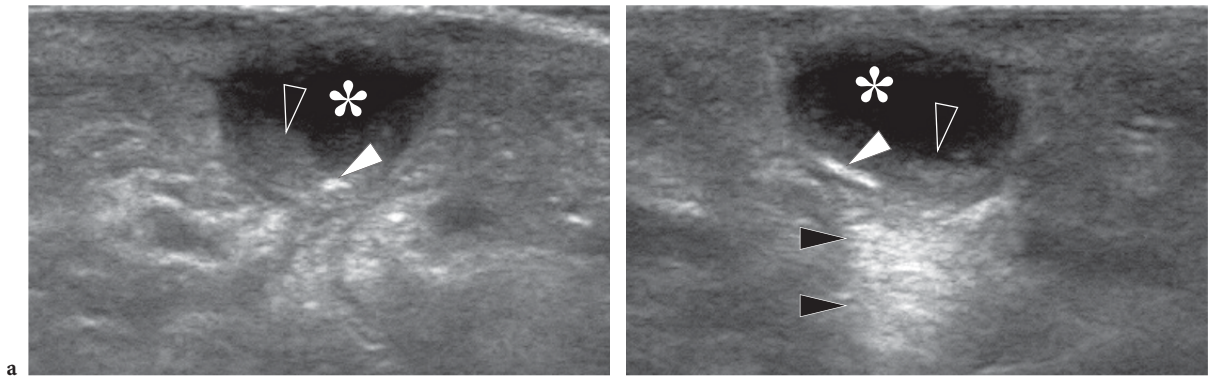

Fig. 2.9a,b. Foreign-body-related abscess. **a** Longitudinal and **b** transverse 12–5 MHz US images over the dorsum of the hand in a patient with signs of local inflammation and a recent open wound. US demonstrates a subcutaneous collection (*asterisk*) with posterior acoustic enhancement (*black arrowheads*) and fluid-debris levels (*open arrowheads*). A small highly reflective foreign body (*white arrowhead*) is contained within the collection. Surgery revealed an abscess containing a small wood splinter

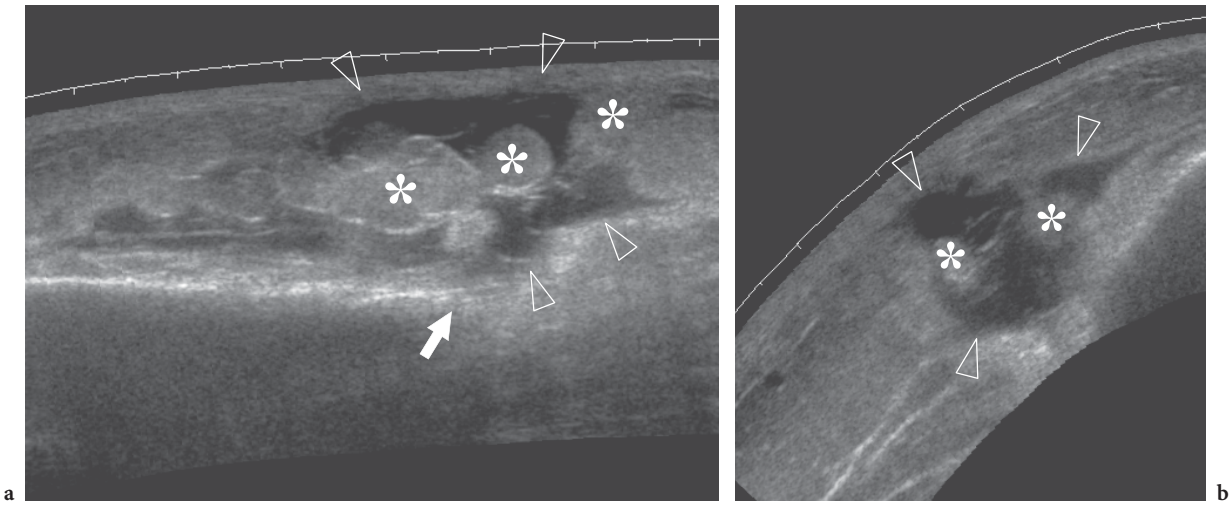

Fig. 2.10a,b. Subcutaneous fat fracture. **a** Transverse and **b** longitudinal 12–5 MHz US images of the gluteal region in a patient with previous local blunt trauma reveal a wide fluid-filled gap (*arrowheads*) representing a subcutaneous fat fracture. Note the disrupted appearance of fatty lobules (*asterisks*) and the alignment of the fracture plane with the edge (*white arrow*) of the iliac bone

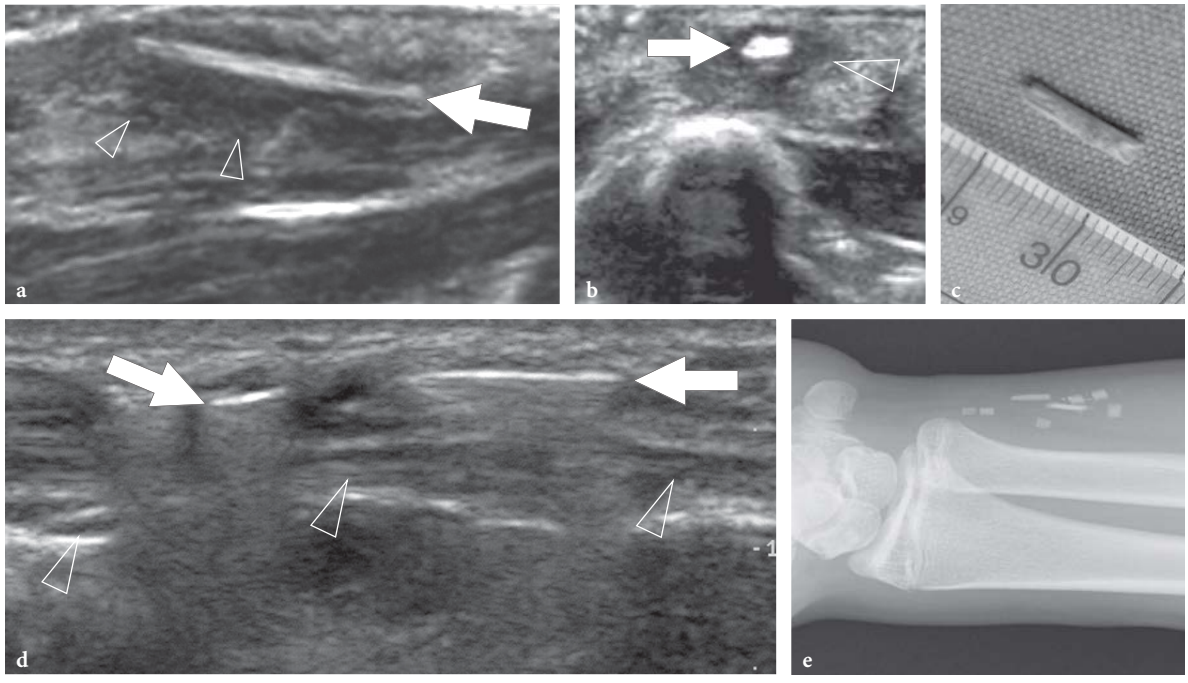

Fig. 2.11a–e. Foreign bodies: US appearance in two patients presenting with **a–c** wood and **d,e** glass fragments. **a** Long-axis and **b** short-axis 12–5 MHz US images of a carpenter who injured his left hand during manual work show an elongated hyperechoic foreign-body (*arrow*) inside the subcutaneous tissue. The fragment is surrounded by a hypoechoic rim (*arrowheads*) representing reactive edema and granulation tissue. **c** At surgery, a wood splinter 1 cm long was removed. **d** Sagittal 12–5 MHz US image of the distal forearm with **e** radiographic correlation in a patient who had an accident during which he broke a glass with his left hand. Initially, physical exploration was negative for foreign bodies and the wound was sutured. At 3 weeks after trauma, US demonstrated two bright linear images (*arrows*) with posterior reverberation (*arrowheads*) reflecting retained glass fragments in the subcutaneous tissue, just superficial to the ulnar nerve (*arrowheads*). **e** Radiographic correlation

lowed by glass and metal fragments (Anderson et al. 1982). Part of them may remain at the site and unrecognized even after apparent successful removal by the patient at the time of the injury (Peterson et al. 2002). If missed, foreign bodies can results in granuloma formation, secondary soft-tissue infection with formation of an abscess, fistula, purulent tenosynovitis and septic arthritis. Bone destructive changes and damage to adjacent nerves may also occur (Choudhari et al. 2001; Peterson et al. 2002). An early diagnosis and prompt removal of foreign bodies is required to prevent complications. Physical examination has intrinsic limitations for detecting and localizing small foreign bodies due to the associated local soft-tissue swelling and pain. It has been reported that approximately 38% of foreign bodies can be overlooked at the initial clinical investigation (Anderson et al. 1982). The deep position of a fragment makes palpation more difficult and less successful. Plain radiography is the initial imaging modality to identify and localize foreign bodies but it can only show radio-opaque fragments: even if very small, metallic fragments are readily detected on plain films. Detection of glass fragments depends on their size and, less importantly, on their lead content, as even if lead-free, almost all glass material is radio-opaque to some degree on radiographs (Felman and Fisher 1969). Radiolucent fragments, such as wood splinters, plant thorns and plastic fragments, cannot be detected by X-rays. Although radiographs allow an estimate of the fragment's location and its relationships with adjacent bones and joints, in relation with tendons, vessels and nerves cannot be investigated. In addition, local complications are not recognized. Xeroradiography and low-kilovoltage radiography have been proposed to increase the detection rate of foreign bodies, but these techniques are currently obsolete.

US is an excellent means of detecting and evaluating post-traumatic foreign bodies (Dean et al. 2003; Soudack et al. 2003; Friedman et al. 2005; Jacobson 2005). In cases of suspected foreign bodies, the examiner should extend the study to a larger area than that closely surrounding the skin wound, as fragments may migrate far away from the entrance point as a result of repeated muscle contraction (Choudhari et al. 2001). As an example, it is not unrealistic to hypothesize that a retained fragment entered the soft tissues on the volar aspect of the wrist may dislocate proximally to reach the anterior distal forearm. As assessed in cadaveric and in vivo studies, the US appearance of foreign bodies varies to a great extent depending on the composition (metal, glass, wood, etc.), shape and site of the fragment (Blyme et al. 1990; Horton et al. 2001). Either radio-opaque or radiolucent fragments can be identified with US as reflective structures with posterior acoustic shadowing or reverberation artifact, depending on the surface characteristics and composition of the foreign body (Boyse et al. 2001; Horton et al. 2001). In general, wood fragments are characterized by posterior acoustic shadowing, whereas glass and metal exhibit reverberations and comet tail artifact (Fig. 2.11). Although these findings lack specificity, they can help to identify foreign bodies as such. Detection of posterior acoustic artifact is particularly helpful for locating tiny fragments that, because of their small size, can go unnoticed. Similarly, a hypoechoic halo surrounding the fragments is of the utmost importance to distinguish them from adjacent soft-tissue structures, such as fat strands or muscles. As assessed in a comparative US-pathologic study, the halo correlates with fibrin, granulation tissue and collagenous capsule formation, whereas the hypervascular pattern seen at color Doppler imaging reflects neovasculature (Davae et al. 2003). The examiner should be aware that US is not accurate for evaluating the fragment's size, as the technique is able only to delineate its surface. On the other hand, the relationship of foreign bodies with adjacent vessels, tendons, muscles and nerves can be precisely assessed. US can recognize a variety of complications, including abscess, granuloma, infectious tenosynovitis and septic arthritis (Fig. 2.12). Generally speaking, the main limitations of this technique occur in the acute phases of trauma, when open wounds or soft-tissue emphysema may make the examination difficult. In an acute setting, care should be taken to avoid contamination of the open wound with gel. In these circumstances, the use of sterile gel and a lateral approach to the skin wound can be recommended to image the fragment. If the foreign body is retained in the distal arm or in the distal leg, US examination can be better performed by placing the affected extremity in a water bath (Blaivas et al. 2004). As determined in an in vitro study, air bubbling can decrease the visibility of foreign bodies, leading to attenuation of the US beam deep to the gas (Lyon et al. 2004). In a preoperative setting, US can identify the foreign body, place a skin mark over it and measure the depth of the fragment relative to the skin. As described in Chapter 18, US can guide the removal of superficial foreign bodies during real-time scanning (Shiels et al. 1990).

In summary, when a foreign body is suspected on clinical grounds, the examiner should briefly

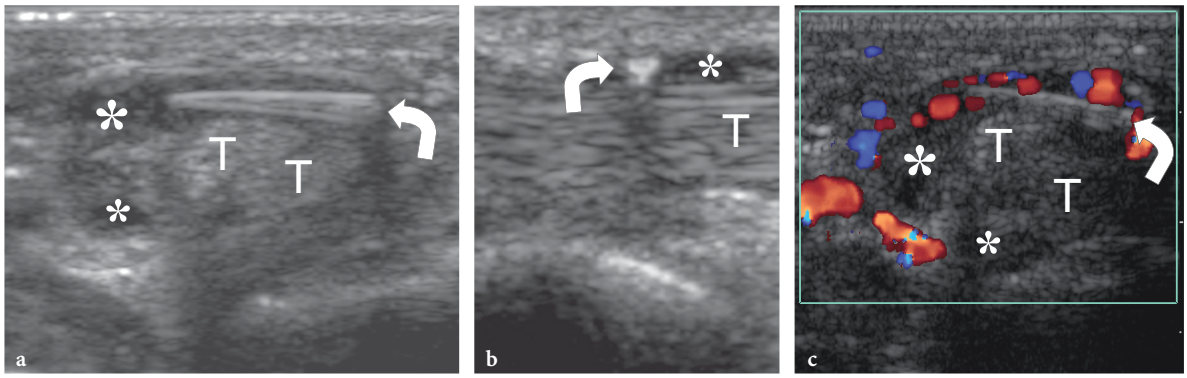

Fig. 2.12a–c. Tenosynovial foreign body. **a** Short-axis and **b** long-axis 15–7 MHz US images over the palm show an elongated wood fragment (*curved arrow*) that has penetrated within the synovial sheath of the flexor tendons (*T*). A thin hypoechoic effusion (*asterisks*) in the tendon sheath allows the fragment to be precisely located in the synovial space. **c** Short-axis color Doppler 15–7 MHz US image reveals a hypervascular flow pattern in the flexor tendon sheath as an expression of reactive hyperemia

discuss the context of trauma with the patient to hear about the nature of possible fragments (glass, wood, metal, etc.). Radiographs should be always performed before US examination. Then, US scanning should cover a wide tissue area around the wound, as foreign bodies may migrate far away from the penetration site. The examiner should seek for bright echoes in the soft tissues but, even more, for structures with posterior acoustic attenuation. Once detected, the fragment should be measured as regards its size, orientation, distance from the skin, and relationships with adjacent tendons, nerves and vessels. Signs of possible infectious complications, such as fluid collections and tenosynovitis, should be annotated as well. Instead of writing a long descriptive report, we prefer to mark the skin overlying the fragment reproducing its size and orientation and to measure the depth of the foreign body: these are important pieces of information for the surgeon before removal. For foreign bodies in deep locations, we recommend appending a drawing to the written report in an effort to better explain the relationship of the foreign body with the adjacent structures.

Orthopaedic implants (screws, pins, etc.) can be found in the soft tissues as a consequence of loosening of orthopaedic devices. Metallic devices appear as bright hyperechoic structures with posterior reverberation artifact (Fig. 2.13). Although they are easily detected on plain films, US allows an excellent analysis of the relationship of loosened implants with adjacent structures, thus helping to plan their removal (Grechenig et al. 1999). Implantable subcutaneous devices are used as long-acting and effective methods of contraception. They consist of a single rod implanted in the subcutaneous tissue of the medial aspect of the arm to release levonorgestrol into the systemic circulation. Based of physical findings, identification of the rod can be difficult if it has inadvertently been inserted too deep or it has migrated away from the insertion point. If removal is required, US is an efficient modality to precisely localize nonpalpable rods, thus allowing their easy removal (Amman et al. 2003; Piessens et al. 2005). Rods appear as a small, elongated, hyperechoic structures with well-defined definite posterior acoustic shadowing, an appearance that correlate well with in vitro findings (Fig. 2.14) (Amman et al. 2003). MR imaging should be used only if US is unrewarding (Merki-Feld et al. 2001). Tissue expanders are widely used in plastic and reconstructive surgery (Neumann 1957). US can assess twisting of injection ports that are surgically inserted into the subcutaneous tissue (Kohler et al. 2005). Twisting is associated with failure of the injection procedure and fluid accumulation in the subcutaneous tissue. US easily demonstrates the upside-down position of the port by showing the linear hyperechoic appearance of the metallic base tilted toward the skin replacing the normal concave superior face of the soft silicone component (Kohler et al. 2005). Suture granulomas may occur after a surgical intervention in which nonabsorbable stitches are used. These tumor-like lesions usually develop slowly and may cause only vague symptoms or remain asymptomatic for many years. US is an accurate way to identify and characterize them by depicting suture material within (Fig. 2.15). As assessed in an in vitro study, the US appearance of surgical sutures is independent of their chemical composition. Monofilament sutures appear as straight bright double lines (like railway

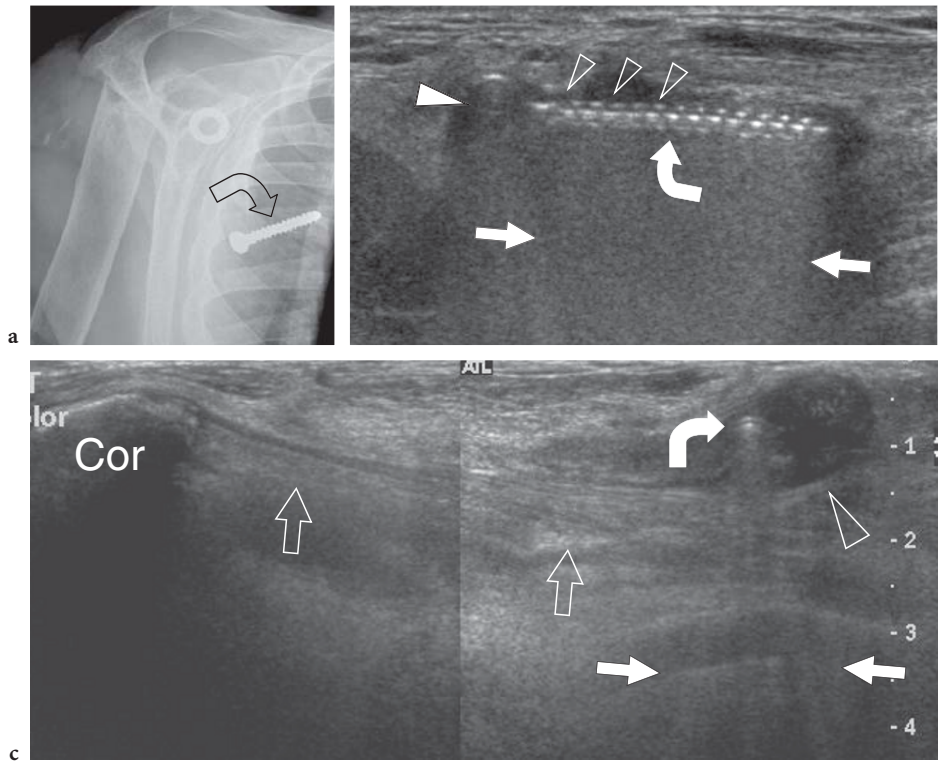

Fig. 2.13a–c. Loosened surgical screw. **a** Anteroposterior radiograph of the shoulder with correlative **b** transverse and **c** split-screen sagittal 12–5 MHz US images over the pectoralis region in a patient with a loosened screw (*curved arrow*) following previous surgery on the shoulder. **a** Radiograph reveals the loosened screw projecting over the right chest but it does not indicate its precise location. **b** At US examination, the screw (*curved arrow*) appears as a hyperechoic structure with posterior reverberation artifact (*straight arrows*) presenting a head (*white arrowhead*) and multiple hyperechoic teeth (*open arrowheads*) at its anterior aspect corresponding to screw spirals. In **c**, the screw appears as a small hyperechoic dot (*curved arrow*) surrounded by fluid collection (*arrowhead*) due to local inflammatory reaction. US allows accurate assessment of the relationship of the screw with the short head of the biceps and the coracobrachialis muscles (*open arrows*) arising from the coracoid (*Cor*)

lines) due to high-amplitude reflection of the US beam at the superficial and deep interface of the suture with the surrounding tissue; braided sutures most often produce a single echo (Rettenbacher et al. 2001). Both patterns show posterior reverberation artifacts. In general, the surrounding granuloma appears as an ill-defined hypoechoic mass, containing a liquefied center where the stitch lies. The main differential diagnoses are granulomas containing other foreign bodies and inflamed epidermoid cysts containing a hair.

2.3.3 Tumors and Tumor-Like Conditions

Soft tissue masses of the subcutaneous tissue include a variety of lesions, such as calcifications, tophaceous gout or rheumatoid nodules, sebaceous cysts and tumors, ranging from the common lipomas and hemangiomas to the rare metastasis and primary malignant masses. Scattered calcifications in the subcutaneous tissue are observed in scleroderma and systemic lupus erythematosus. They appear as mottled hyperechoic lesions with posterior acoustic shadowing. US has little value in their assessment as they are manifest on plain films. Subcutaneous calcifications are often the result of drug injections. For the most part, they are encountered in the buttock and appear as well-delimited hyperechoic structures with strong posterior acoustic shadowing (Fig. 2.16a). In rheumatologic patients, subcutaneous nodules are mainly due to tophaceous gout or rheumatoid nodules (Tiliakos et al. 1982; Benson et al. 1983; Nalbant et al. 2003). Tophi are soft-tissue agglomerates of uric acid crystals that can develop in different areas of the body: the hand, the foot and the elbow the most commonly involved.

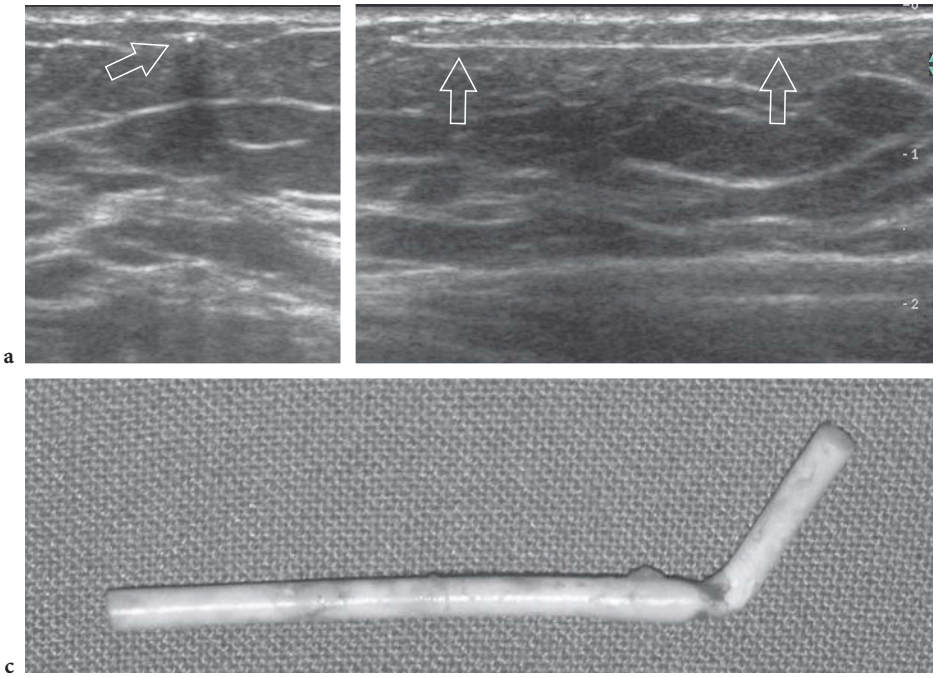

Fig. 2.14a–c. Subdermal contraceptive device (Implanon). **a** Short-axis and **b** long-axis 12–5 MHz US images over a flexible subdermal plastic implant (*arrows*) for long-acting release of synthetic hormones. In selected cases, US can assist in the localization and minimally invasive removal of the implant. **c** Photograph of an Implanon rod after surgical removal

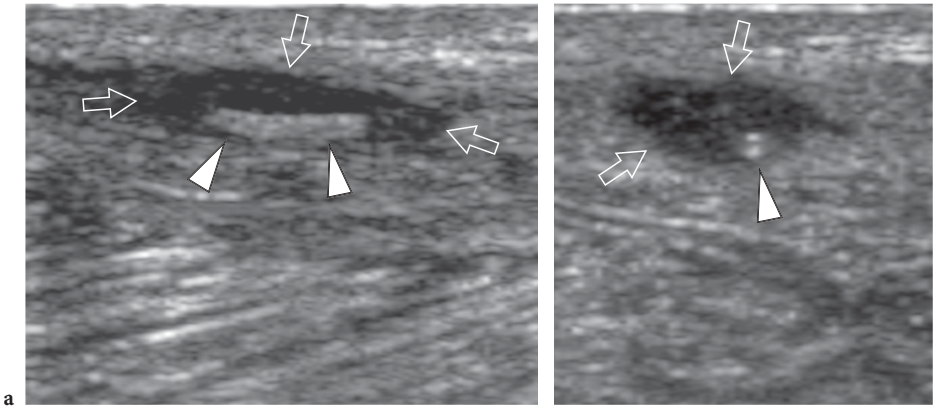

Fig. 2.15a,b. Suture granuloma. **a** Long-axis and **b** short-axis 12–5 MHz US images show a suture granuloma located in the lower abdominal wall after inguinal herniorrhaphy. Within the hypoechoic granuloma (*arrows*), the surgical suture appears as a hyperechoic rail-like line (*arrowheads*) when imaged in its long-axis. On the short-axis image, the suture assumes the appearance of a double dot (*arrowhead*)

At US examination, tophi appear as heterogeneous masses containing hypoechoic areas related to chalky liquid material surrounded by hyperechoic tissue (Nalbant et al. 2003). Rarely, calcific deposits can be detected within the tophaceous mass in the form of hyperechoic spots with or without posterior acoustic attenuation (Fig. 2.16b) (Gerster et al. 2002). Rheumatoid nodules occur in 20–30% of rheumatoid patients who have a high serum level of rheumatoid factor and active articular disease (McGrath and Fleisher, 1989). They seem to derive from an immune complex process between rheumatoid factor and immunoglobulin G initiating small vessel abnormalities and then progressing to necrosis and granulation tissue. Gross examination of these nodules reveals a semifluid center sur-

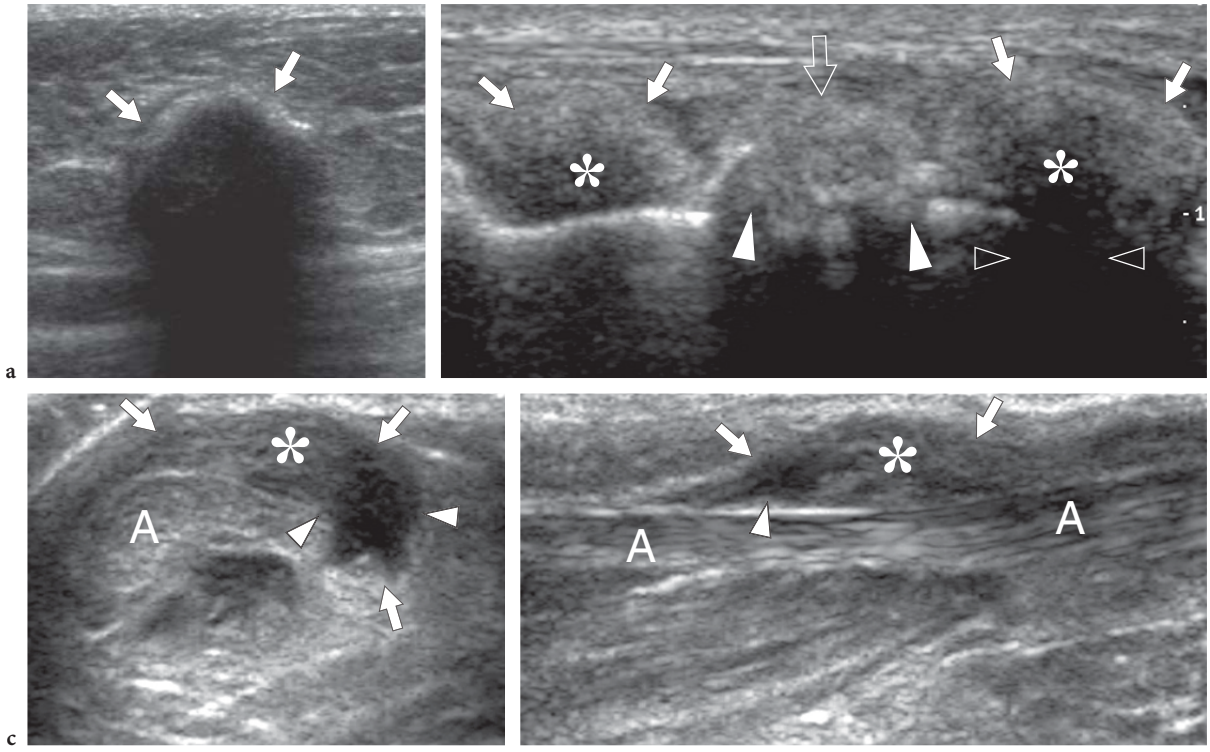

Fig. 2.16a–d. Non-neoplastic subcutaneous masses. **a** Elaioma. Transverse 12–5 MHz US image demonstrates dystrophic calcification (*arrows*) in the subcutaneous tissue of the buttock, at the site of previous injection therapy. **b** Tophaceous gout. Longitudinal 12–5 MHz US image over the forefoot reveals tophi as para-articular ill-defined hypoechoic masses (*asterisks*) with posterior acoustic shadowing (*open arrowheads*) and hyperechoic surrounding halo (*arrows*), adjacent to the MIP joint. Note the osteoarthritic changes (*white arrowheads*) in the underlying joint. **c,d** Rheumatoid nodules. **c** Transverse and **d** longitudinal 12-5 MHz US images over the Achilles tendon (*A*) in an HIV-positive patient affected by longstanding rheumatoid arthritis show a rheumatoid nodule as a hypoechoic mass (*arrows*) arising from the paratenon and growing into the subcutaneous tissue. The nodule has a mixed echotexture with solid (*asterisk*) and fluid (*arrowheads*) components

rounded by dense connective tissue. Rheumatoid nodules are usually found at pressure sites, such as the extensor aspect of the elbow, the fingers and the calcaneus, and correlate with a bad prognosis. US displays hypoechoic masses with a central sharply demarcated hypoechoic area reflecting necrosis (Fig. 2.16c,d) (Nalbant et al. 2003).

2.3.3.1 Lipomas

Superficial lipomas typically appear as compressible, palpable soft-tissue masses in the subcutaneous tissue not adherent with the overlying skin. Lipomas have a male and familial predominance and tend to grow in the back, shoulder and upper arms with a predilection for the extensor surface. They are more common in the fifth and sixth decades. Although lipomas most often present as a solitary oval or rounded mass, they may be multiple (5%–15%) (Murphey et al. 2004). At US examination, lipomas have a wide range of appearances. Typically, they present as elliptical compressible masses containing short linear reflective striations that run parallel to the skin (Fig. 2.17a). However, their internal echogenicity may vary from hyperechoic to hypoechoic or mixed relative to muscle depending on the degree of connective tissue and other reflective interfaces – such as cellularity, fat and water – within the mass (Fornage and Tassin 1991; Ahuja et al. 1998). At least theoretically, it has been postulated that lipomas composed of pure fat should be echo-free lesions due to a low number of tissue acoustic interfaces (Behan and Kazam 1978). Based on different series, the incidence of hyperechoic lipomas, reflecting the so-called fibrolipomas, varies from 20% to 76% (Fornage and Tassin 1991; Ahuja et al. 1998; Inampudi et al. 2004). In a recent retrospective review of 39 US-diagnosed superficial and

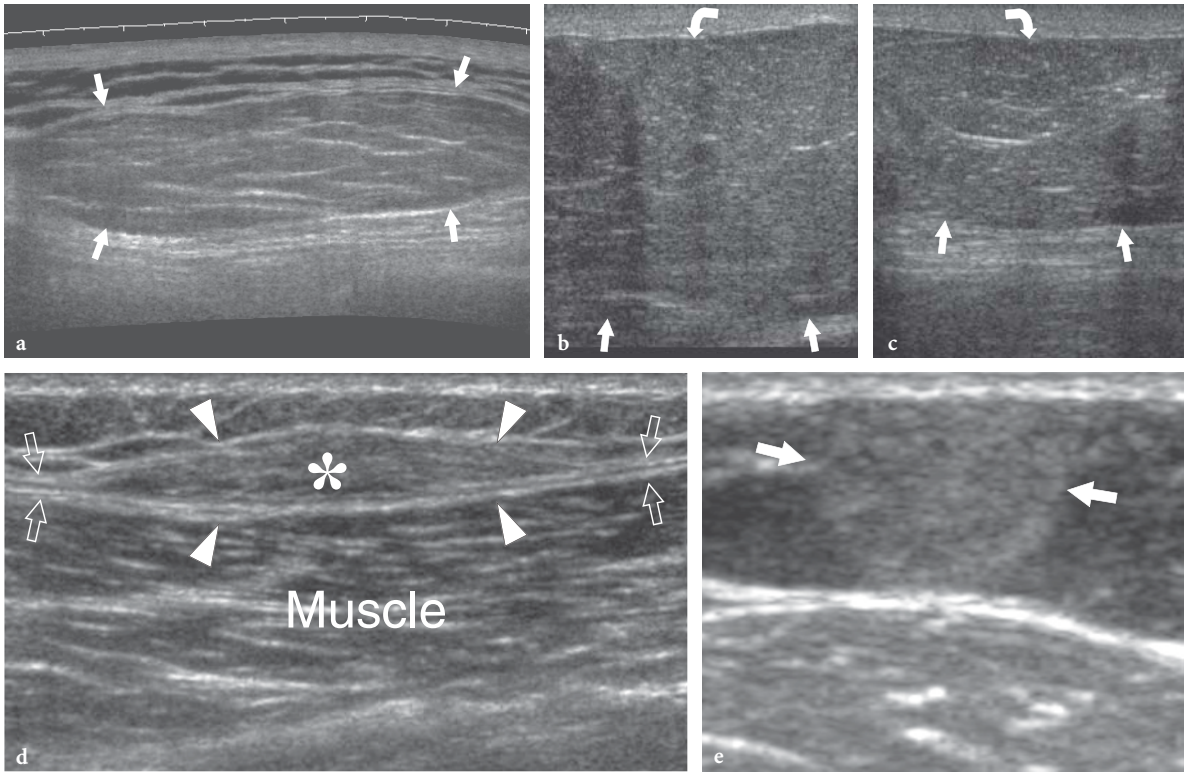

Fig. 2.17a–e. Subcutaneous lipoma: spectrum of typical US appearances. **a** Long-axis extended-field-of-view 12–5 MHz US image of a lipoma of the back shows an elongated well-defined compressible mass with its greatest diameter parallel to the skin. The mass has well-defined margins and appears slightly hyperechoic relative to adjacent fat. Its echotexture consists of short thin linear striations that run parallel to the skin. **b** Long-axis 12–5 MHz US image at the border of a nonencapsulated lipoma (*arrows*) in a patient with a palpable mass at the medial aspect of the left thigh with **c** correlative contralateral image. **d** Long-axis 12–5 MHz US image of an intrafascial lipoma shows a lenticular fatty mass (*asterisk*) contained in a split of the muscle fascia (*arrows*). Note the fascia dividing into two hyperechoic sheets (*arrowheads*) to envelop the lipoma. **e** Transverse 12–5 MHz US image of the left forearm in patient with pathologically-proven angiolipoma demonstrates a hyperechoic rounded mass (*arrows*) with small internal hypoechoic dots

deep-seated lipomas, histologic diagnosis revealed 25 lipomas and 14 nonlipomas, including other benign and malignant histotypes (Inampudi et al. 2004). This indicates that the variable echotexture of lipomas may make their differentiation from other masses subjectively difficult. Although many lipomas have a well-circumscribed appearance with an identifiable thin capsule, a significant proportion (12%–60%) have ill-defined borders blending imperceptibly with the surrounding subcutaneous fat (Fig. 2.17b,c) (Fornage and Tassin 1991; Ahuja et al. 1998; Inampudi et al. 2004). This may lead to difficulties in identifying them with US even if the mass is apparent clinically. Nonencapsulated lipomas may require comparison with the contralateral side to detect significant asymmetry of fat tissue. They should be referred to as "probable lipomas" in the report as long as there are corroborative clinical findings of a discrete mass (Roberts et al. 2003).

In daily practice, the occurrence of a superficial palpable lump suggesting a lipoma in the absence of a definite nodule detectable with US is not uncommon. Graded compression with the probe or combined imaging and palpation may be helpful for detecting these "occult" lipomas. Both maneuvers can increase the detection rate of the mass, which is less compressible than the adjacent subcutaneous tissue. Most superficial lipomas do not present substantial internal vasculature at color and power Doppler imaging, a finding that may enhance the confidence of the examiner that a benign mass is present (Ahuja et al. 1998). Some lipomas grow in the deep subcutaneous tissue, in close contact with the fascia. Care should be taken when reporting on these masses not to lead the surgeon to believe that the lesion can be easily excised, because deep subcutaneous lipomas may adhere to the fascia. A well-delimited mass does not always mean an easily

removable lesion. Lipomas growing inside the deep fascia may also occur. The clinical diagnosis of these lesions may be difficult because they are firm and tethered to the deep plane and may mimic more aggressive tumors. At US examination, intrafascial lipomas appear as lenticular lesions growing into a split of the fascia, which retains a normal hyperechoic appearance (Fig. 2.17d). In these cases, US can rule out abnormalities of the underlying muscles and aggressive growth patterns suggestive of a malignant tumor.

Lipomas containing other mesenchymal elements, such as fibrous tissue (fibrous lipomas), cartilage (chondroid lipomas), mucoid component (myxolipoma) and vessels (angiolipoma), may be encountered. In these cases, the presence of nonlipomatous elements may make the US appearance of the lesion less specific. Among these variants, angiolipomas account for 5%–17% of all lipomas (Lin and Lin 1974). They are well-defined hyperechoic subcutaneous masses containing small patchy hypoechoic areas and sparse internal vasculature (Fig. 2.17e) (Choong 2004). Relative to lipomas, angiolipomas have a greater angiomatous component composed of thin-walled capillaries which account for up to 90% or more of the lesion, and occur at an earlier age (early adulthood). Hibernomas (fetal lipomas) are rare benign tumors composed of brown fat. Brown fat is histologically distinct from white adipose tissue and plays a role in nonshivering thermogenesis of hibernating animals and newborn humans. In humans, brown adipose tissue progressively decreases through adulthood. Usual locations of tumors arising from brown fat are the parascapular and interscapular spaces, the mediastinum, the upper thorax and the thighs. US demonstrates a solid well-marginated hyperechoic mass somewhat resembling a lipomatous tumor and Doppler imaging may show a hypervascular pattern reflecting the presence of vascular structures and the increased cellular metabolism of hibernomas. Other rare forms of lipomas, including lipomatosis of nerves (see Chap. 4) and lipoma arborescens (see Chap. 14) are described elsewhere.

Other space-occupying nonlipomatous masses containing fat may mimic the US appearance of lipomas. Among them, hemangiomas contain a variable amount of adipose tissue interspersed between abnormal vessels. However, in most cases their typical US appearance made of serpentine or tubular hypoechoic structures contained within the mass, scattered phleboliths and prominent blood flow at color and power Doppler imaging, allows the correct diagnosis to be made.

Lipomatosis represents a diffuse overgrowth of mature adipose tissue histologically similar to simple lipomas. The fatty tissue extensively infiltrates the subcutaneous and muscular tissue and is not associated with nerve involvement. Many entities of superficial lipomatosis are described (Murphey et al. 2004). In multiple symmetric lipomatosis, which is commonly referred to as Madelung or Launois-Bensaude lipomatosis, multiple symmetric lipomas are found in the neck and the shoulder in association with alcoholism, hepatic disease and metabolic disorders (Uglesic et al. 2004). Dercum disease, which is also referred to as lipomatosis dolorosa or adiposis dolorosa, is a rare disorder occurring in middle-aged women, often obese, in which multiple painful subcutaneous lipomas occur (Wortham and Tomlinson 2005).

2.3.3.2 Pilomatricoma and Epidermal Inclusion (Sebaceous) Cysts

Pilomatricoma (pilomatrixoma), also called calcifying epithelioma of Malherbe, is a benign superficial tumor of the hair follicle arising from the hair cortex cells in the deep dermis and extending into subcutaneous tissue as it grows (Malherbe and Chemantais, 1880). Most lesions arise in children less of 10 years of age and appear as small masses (<3 cm in diameter) with a rock-hard consistency and an irregular surface, which causes skin stretching over the mass (Hwang et al. 2005). Although the overall incidence of pilomatricoma is low, it is one of the most commonly excised superficial masses in children with epidermoid cysts. Preferential anatomic sites of pilomatricomas are the neck, the cheek, the preauricular area and the extremities, including arm and leg. US demonstrates pilomatricomas as hyperechoic masses relative to the muscle with posterior acoustic shadowing reflecting internal calcification or ossification (Fig. 2.18a) (Hwang et al. 2005). The amount and shape of calcification may vary from few scattered echogenic foci to gross clumped deposits within the mass or a completely calcified nodule. In most cases, a peripheral hypoechoic rim surrounding the calcific deposits is observed (Hwang et al. 2005). Peripheral color Doppler flow is often found in the peripheral region of the mass.

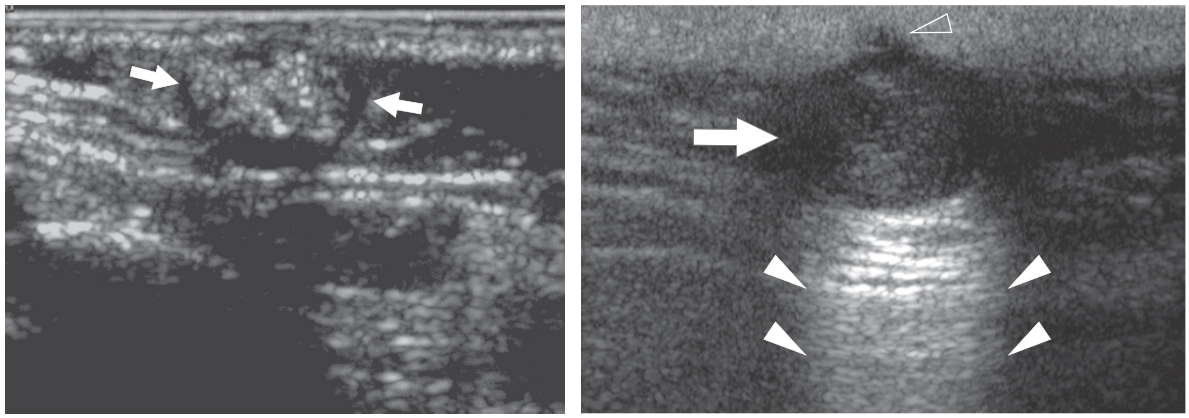

Fig. 2.18a,b. Epidermal-related masses. **a** Pilomatricoma. Transverse 10–5 MHz US image in a child with a stiff superficial lump in the preauricular area reveals a mass (*arrows*) characterized by a peripheral hypoechoic rim and a hyperechoic center with scattered calcified foci causing posterior acoustic attenuation. **b** Epidermal inclusion cyst. US demonstrates a rounded hypoechoic mass (*arrow*) with posterior acoustic enhancement (*white arrowheads*) and a small superficial extension into the dermis (*open arrowhead*)

Epidermal inclusion cysts, which are also referred to as sebaceous, epidermoid, epidermal, infundibular or keratin cysts, derive from the focal proliferation of epidermal cells within the subcutaneous tissue. The theory that these cysts may develop from the subcutaneous implantation of keratinizing epithelial elements during embryogenesis or a previous trauma or surgery is widely accepted. Sebaceous cysts most often arise from swollen sebaceous glands or hair follicles and are limited to the skin surfaces in which sebaceous glands are present (i.e., the dorsal but not the ventral aspect of the hand). Epidermal inclusion cysts are lined with epithelial cells and filled with a white, cheesy material reflecting layers of keratin and cholesterol-rich debris. Clinically, epidermal inclusion cysts present as slow-growing, freely movable lumps beneath the skin. They usually remain asymptomatic unless they become infected, grow large enough to interfere with normal function, or rupture into the adjacent soft tissues. US shows epidermal cysts as ovoid or spherical sharply bordered hypoechoic masses with scattered echoes presenting posterior acoustic enhancement and a small extension into the dermis corresponding to their small opening that communicates with the skin (Fig. 2.18b) (Lee et al. 2001). However, the internal echogenicity of epidermoid inclusion cysts may vary depending on the hydration of the keratin, protein composition and microcalcifications (Fig. 2.19) (Vincent et al. 1985; Lee et al. 2001). The typical "onion-ring" (bull's-eye) appearance described in the testis as a result of multiple layers of keratin debris is usually not observed in epidermal cysts arising from soft tissues (Brenner et al. 1989; Maxwell and Mamtora 1990). Ruptured cysts may assume a lobulated or irregular contour as a result of intense granulomatous reaction and show color Doppler signals, possibly mimicking a neoplasm (Lee et al. 2001).

2.3.3.3 Hemangiomas and Vascular Malformations

Even though the term "hemangioma" is often used in a general way to encompass both hemangiomas and vascular malformations, hemangiomas represent endothelial-lined neoplasms that mainly occur in childhood, growing to reach a maximum volume and then regress, whereas vascular malformations are composed of dysplastic vessels which show no cellular proliferation or regression. Hemangiomas can be categorized into capillary and cavernous types, whereas vascular malformations may be divided in high-flow, slow-flow and capillary lesions. Hemangiomas may be hypoechoic or hyperechoic relative to surrounding tissue and may have a homogeneous or complex appearance (Fig. 2.20a). High vessel density and high peak arterial Doppler shifts (>2 kHz) are typically observed and help in distinguishing hemangiomas from other soft-tissue masses (Fig. 2.20b–f) (Dubois et al. 1998, 2002). High-flow malformations are typified by an abnormal network of vascular channels (the nidus), interposed between a prominent feeding artery and a dilated draining

Fig. 2.19a–d. Epidermal inclusion cyst. **a** Lateral radiograph of the middle finger in a patient with a palpable mass on the ventral aspect of the proximal phalanx reveals a superficcial oval soft-tissue mass (*arrows*). **b** Transverse 12–5 MHz color Doppler US image of the affected finger demonstrates a well-circumscribed hypovascular mass (*arrows*) characterized by a homogeneous texture of medium-level echoes in close relationship with the flexor tendons (*T*). Correlative **c** fat-suppressed T2-weighted and **d** gadolinium-enhanced fat-suppressed T1-weighted MR images show a homogeneous lesion (*arrow*) of high signal intensity on T2-weighted images, central non-enhancement and peripheral thin rim enhancement. Surgery revealed an epidermal inclusion cyst

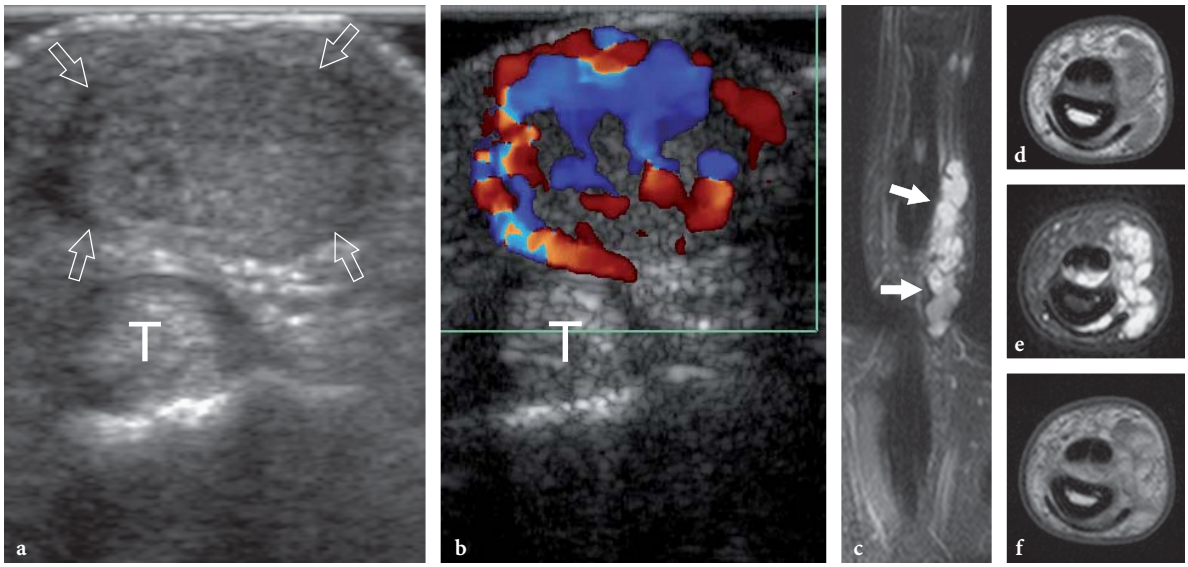

Fig. 2.20a–f. Hemangioma. Transverse **a** gray-scale and **b** color Doppler 15–7 MHz US images of the index finger in a patient with an indolent palpable mass demonstrate a well-circumscribed solid hypoechoic nodule (*arrows*) located just superficial to the flexor tendons (*T*). The mass reveals several intratumoral vessels. **c** Coronal fat-suppressed T2-weighted and transverse **d** T1-weighted, **e** fat-suppressed T2-weighted and **f** gadolinium-enhanced T1-weighted MR imaging correlation

vein. Spectral Doppler analysis demonstrates high systolic arterial flow and arterialization of the veins (Fig. 2.21) (Dubois et al. 1999). Slow-flow (venous) malformations are characterized by abnormally dilated venous spaces and a normal arterial component. Often, they may be suspected on the basis of a subcutaneous bluish or reddish stain. In approximately 15% of cases they contain phleboliths (calcifications in venous thrombosis), which can be seen as hyperechoic foci with posterior acoustic shadowing (Fig. 2.22). Due to slow blood flow, color Doppler imaging may detect only sparse monophasic flow or no blood flow signals at all (Trop et al. 1999). Distinguishing between a slow-flow malformation and an involuted hemangioma may be problematic. In general, vascular malformations are distinguished from hemangiomas owing to the absence of solid tissue (Paltiel et al. 2000). In addition, hemangiomas have similar vessel density and peak systolic velocities but lower venous velocity (Paltiel et al. 2000). Finally, there are capillary malformations limited to the dermis. For the most part, US is unable to display such superficial abnormalities that typically present with a port-wine like stain. In some instances, however, an increased thickness of the subcutaneous tissue and some prominent veins may be demonstrated.

2.3.3.4 Metastases and Lymphomas

Superficial metastases involving the skin and subcutaneous tissue account for approximately 0.5%–9% of tumors. They usually result from seeding of deep tumors during interventional (i.e., needle and surgical biopsy) or surgical procedures or represent a manifestation of end-stage cancer (Galarza and Sosa 2003). In some cases, however, skin metastases can be the first manifestation of an occult cancer, therefore requiring an accurate and early diagnosis (Giovagnorio et al. 2003). Histopathologically, metastases of the skin and subcutaneous tissue can develop from almost any kind of malignancy, but nearly half of them derive from melanoma, lung cancer and breast carcinoma (White 1985). In most cases, metastases appear as well-circumscribed solid hypoechoic masses (Nazarian et al. 1998). A lobulated shape and multiple peripheral vascular pedicles feeding internal irregular vessels seem the most important gray-scale and color Doppler US imaging findings for differentiating them from other benign soft-tissue masses (Fig. 2.23) (Giovagnorio et al. 1999, 2003). In follow-up studies, color Doppler imaging has been proposed as a mean to assess the pharmacodynamic response to chemotherapy

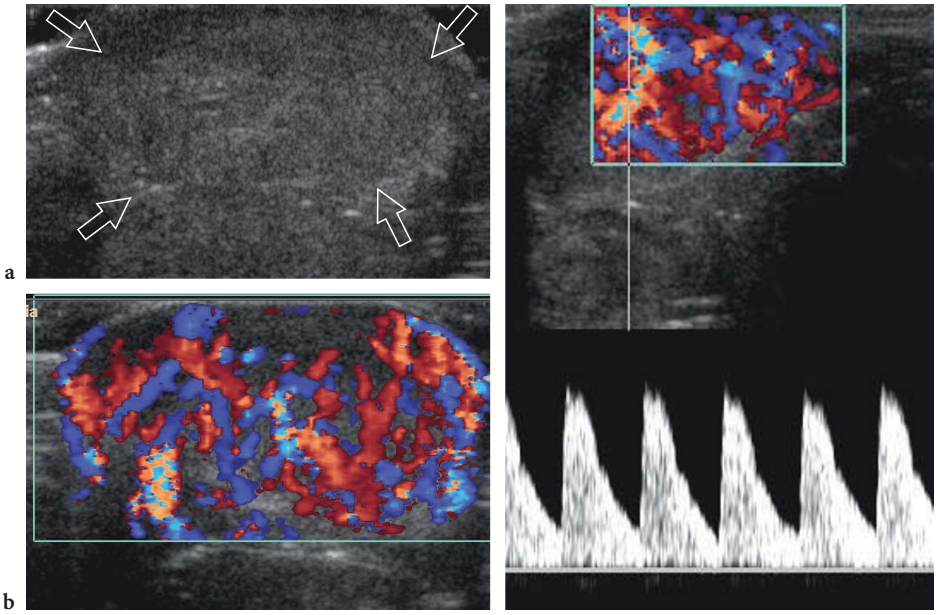

Fig. 2.21a–c. Arteriovenous malformation. **a** Transverse gray-scale 15–7-MHz US image of a 6-month-old infant born with a markedly swollen cheek and upper lip reveals marked thickening of the subcutaneous tissue of the lip (*arrows*). **b** Corresponding color Doppler 15–7 MHz US image demonstrates numerous enlarged vessels coursing through the thickened subcutaneous tissue. **c** Spectral Doppler analysis demonstrates high-velocity arterial waveforms within the vessels

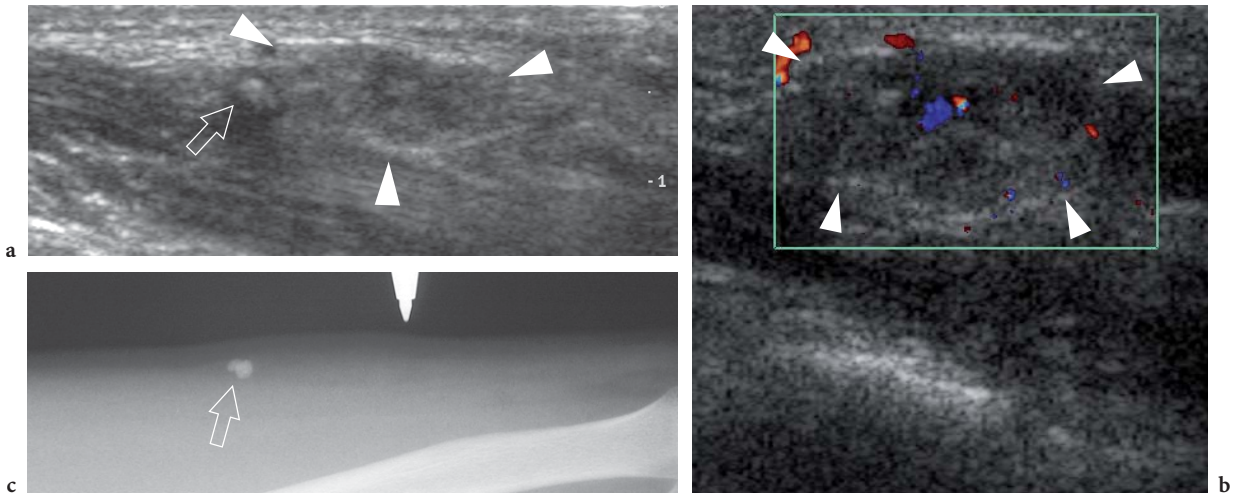

Fig. 2.22a–c. Venous malformation. **a** Longitudinal 12–5 MHz US image of the middle forearm show an ill-defined sponge-like subcutaneous mass (*arrowheads*) containing a network of anechoic channels and a hyperechoic dot (*arrow*) with posterior acoustic shadowing, likely reflecting a phlebolith. **b** Corresponding 12–5 MHz color Doppler US image reveals only a few, weak signals of flow within the soft-tissue mass (*arrowheads*). **c** Radiographic correlation confirms the presence of a few rounded phleboliths (*arrow*) within the lesion

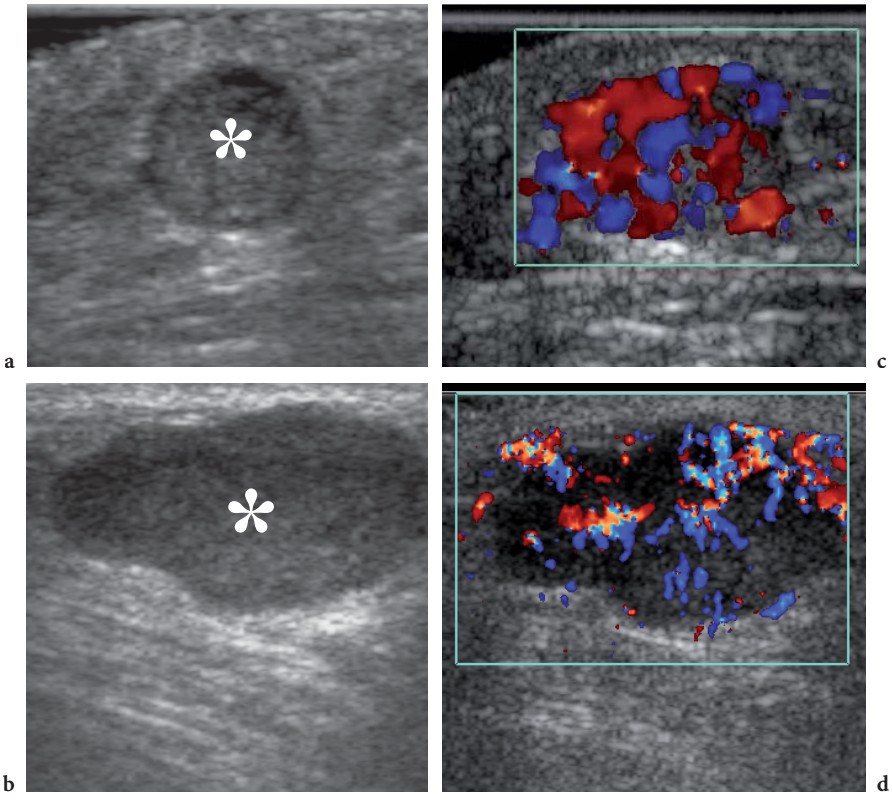

Fig. 2.23a–c. Subcutaneous tissue metastases. **a,b** Gray-scale and **c,d** color Doppler 12–5 MHz US images in two patients with previously diagnosed malignancies demonstrate well-defined homogeneous hypoechoic nodules (*asterisk*) located within the subcutaneous tissue. In both nodules, correlative color Doppler imaging shows a hypervascular pattern with peripheral and internal vessels. Postsurgical histologic examination revealed metastases from **a,c** gut carcinoma and **b,d** colon adenocarcinoma

by depicting reduction of intratumoral blood flow (Fig. 2.24) (Nazarian et al. 1996). In patients operated on for melanoma, detection of any nonpalpable mass in the subcutaneous tissue or any suspected regional lymphadenopathy should be ascertained by means of US-guided biopsy (Fornage and Lorigan 1989).

The subcutaneous tissue can be the primary site of involvement of peripheral T-cell (non-Hodgkin) lymphoma (Lee et al. 2003; Fujii et al. 2004; Giovagnorio 1997). This kind of lymphoma involves the skin and the subcutaneous tissue in two main forms: the cutaneous T-cell lymphoma, which is also known as mycosis fungoides or Sézary syndrome, and the subcutaneous panniculitis-like T-cell lymphoma (Lee et al. 2003). Mycosis fungoides is an indolent disorder presenting with cutaneous patches, plaques or erythroderma. With time, the skin lesions may progress to cutaneous tumors, peripheral lymphadenopathies and widespread extracutaneous involvement, with a corresponding drop in patient survival rate. At the stage of tumor formation, US is able to demonstrate diffuse or focal hypoechoic thickening of the skin; the imaging features of this lymphoma are, however, nonspecific (see Fig. 2.3a) (Fornage et al. 1993). The subcutaneous panniculitis-like T-cell lymphoma is a rare condition which may be a diagnostic challenge as it mimics inflammatory cellulitis associated with connective tissue disease (Lee et al. 2003; Sy et al. 2005). This disorder usually presents with multiple

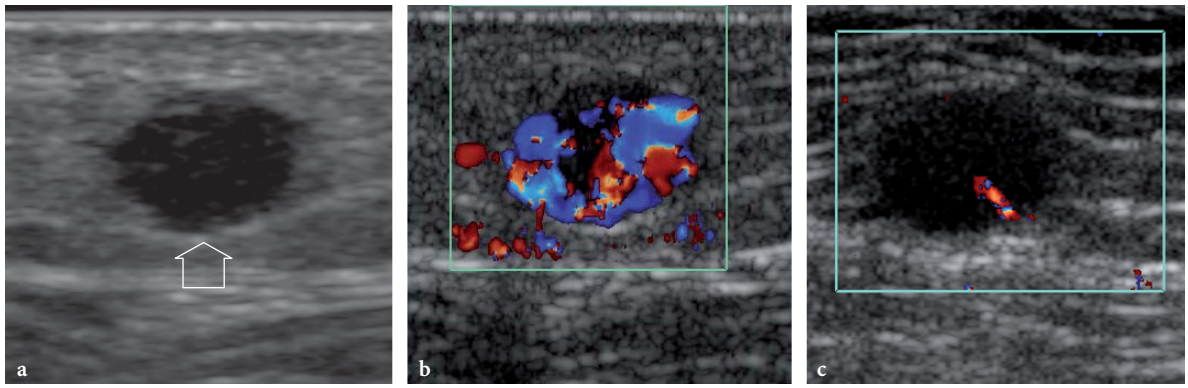

Fig. 2.24a–c. Subcutaneous regional metastasis from melanoma. **a** Gray-scale and **b,c** color Doppler 15–7 MHz US images in a patient who had a melanoma in his left foot and some regional relapses reveal a small solid homogeneously hypoechoic nodule (*arrow*) with spiculated margins in the subcutaneous tissue of the left lower leg. The nodule is hypervascular at color Doppler imaging. **c** After a course of systemic chemotherapy and immunotherapy, the subcutaneous metastasis appears unchanged in size and echotexture but assumes a hypovascular pattern reflecting therapy-related change in tumor perfusion

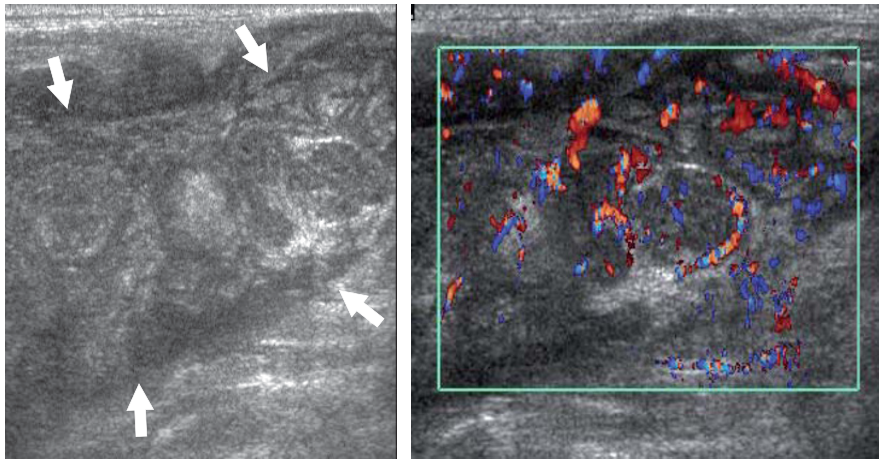

Fig. 2.25a,b. Subcutaneous panniculitis-like T-cell lymphoma. **a** Gray-scale and **b** color Doppler 12–5 MHz US images over an hardened ill-defined area in the back show diffuse pseudonodular thickening of the subcutaneous tissue (*arrows*) with a generalized decrease in echogenicity of the fat lobules and a diffuse hypervascular pattern mimicking cellulitis

palpable subcutaneous nodules, and may undergo rapid deterioration secondary to the onset of the hemophagocytic syndrome (marked anemia due to phagocytosis of red blood cells from monocytes and macrophages). US reveals marked increased echogenicity with swelling of the fat lobules and blurry differentiation between the skin and the subcutaneous tissue, an appearance resembling a diffuse inflammatory infiltrate with edema (Fig. 2.25) (Sy et al. 2005). Hypoechoic nodules surrounded by a hyperechoic rim can also be observed (Fujii et al. 2004). Given the similarity with inflammatory cellulitis, regional enlarged lymph nodes could possibly be misinterpreted as reactive in nature (Sy et al. 2005).

References

Ahuja AT, King AD, Kew J et al (1998) Head and neck lipomas: sonographic appearances. AJNR Am J Neuroradiol 19: 505–508

Akesson A, Forsberg L, Hederstrom E (1986) Ultrasound examination of skin thickness in patients with progressive systemic sclerosis (scleroderma). Acta Radiol Diagn 27: 91–94

Amann P, Botta U, Montet X et al (2003) Sonographic detection and localization of a clinically nondetectable subcutaneous contraceptive implant. J Ultrasound Med 22: 855–859

Anderson MA, Newmeyer WL 3rd, Kilgore ES Jr (1982) Diagnosis and treatment of retained foreign bodies in the hand. Am J Surg 144: 63–67

Arslan H, Sakarya ME, Bozkurt M et al (1998) The role of power Doppler sonography in the evaluation of superficial soft tissue abscesses. Eur J Ultrasound 8: 101–106

Behan M, Kazam E (1978) The echographic characteristics of fatty tissues and tumors. Radiology 129: 143–151

Benson CH, Gibson JY, Harisdangkul V (1983) Ultrasound diagnosis of tophaceous and rheumatoid nodules. Arthritis Rheum 26: 696

Blaivas M, Lyon M, Brannam L et al (2004) Water bath evaluation technique for emergency ultrasound of painful superficial structures. Am J Emerg Med 22: 589–593

Blyme PJ, Lind T, Schantz K et al (1990). Ultrasonographic detection of foreign bodies in soft tissue: a human cadaver study. Arch Orthop Trauma Surg 110: 24–25

Boyse TD, Fessell DP, Jacobson JA et al (2001) US of soft-tissue foreign bodies and associated complications with surgical correlation. RadioGraphics 21: 1251–1256

Brenner JS, Cumming WA, Ros PR (1989) Testicular epidermoid cyst: Sonographic and MR findings. AJR Am J Roentgenol 152: 1344

Brocks K, Stender I, Karlsmark T et al (2000) Ultrasonic measurement of skin thickness in patients with systemic sclerosis. Acta Derm Venereol 80: 59–60

Canturk F, Canturk T, Aydin F et al (2004) Cutaneous linear atrophy following intralesional corticosteroid injection in the treatment of tendonitis. Cutis 73: 197–198

Cardinal E, Bureau N, Aubin B et al (2001) Role of ultrasound in musculoskeletal infection. Radiol Clin North Am 39: 191–201

Chau CL, Griffith JF (2005) Musculoskeletal infections: ultrasound appearances. Clin Radiol 60: 49–59

Choong KKL (2004) Sonographic appearance of subcutaneous angiolipomas. J Ultrasound Med 23: 715–717

Choudhari KA, Muthu T, Tan MH (2001) Progressive ulnar neuropathy caused by delayed migration of a foreign body. Br J Neurosurg 15: 263–265

Clements PJ, Hurwitz EL, Wong WK et al (2000) Skin thickness score as a predictor and correlate of outcome in systemic sclerosis. Arthritis Rheum 43: 2445–2454

Davae KC, Sofka CM, DiCarlo E et al (2003) Value of power Doppler imaging and the hypoechoic halo in the sonographic detection of foreign bodies: correlation with histopathologic findings. J Ultrasound Med 22: 1309–1313

Dean AJ, Gronczewski CA, Costantino TG (2003) Technique for emergency medicine bedside ultrasound identification of a radiolucent foreign body. J Emerg Med 24: 303–308

Dubois J, Garel L (1999) Imaging and therapeutic approach of hemangiomas and vascular malformations in the pediatric age group. Pediatr Radiol 29: 879–893

Dubois J, Patriquin HB, Garel L et al (1998) Soft-tissue hemangiomas in children and infants: diagnosis using Doppler ultrasonography. AJR Am J Roentgenol 171: 247–252

Dubois J, Garel L. David M et al (2002) Vascular soft-tissue tumors in infancy: distinguishing features on Doppler sonography. AJR Am J Roentgenol 178: 1541–1545

Ehara S (1998) MR imaging of fat necrosis. AJR Am J Roentgenol 171: 889

Erickson SJ (1997) High-resolution imaging of the musculoskeletal system. Radiology 205: 593–618

Felman AH, Fisher MS (1969) The radiographic detection of glass in soft tissue. Radiology 92: 1529–1531

Fernando RA, Somers S, Edmonson RD et al (2003) Subcutaneous fat necrosis: hypoechoic appearance on sonography. J Ultrasound Med 22: 1387–1390

Fornage BD, Deshayes JL (1986) Ultrasound of normal skin. J Clin Ultrasound 14: 619–622

Fornage BD, Lorigan JG (1989) Sonographic detection and fine-needle aspiration biopsy of nonpalpable recurrent or metastatic melanoma in subcutaneous tissues. J Ultrasound Med 8: 421–424

Fornage BD, Tassin GB (1991) Sonographic appearances of superficial soft tissue lipomas. J Clin Ultrasound 19: 215–220

Fornage BD, McGavran MH, Duvic M et al (1993) Imaging of the skin with 20-MHz US. Radiology 189: 69–76

Friedman DI, Forti RJ, Wall SP et al (2005) The utility of bedside ultrasound and patient perception in detecting soft tissue foreign bodies in children. Pediatr Emerg Care 21: 487–492

Fujii Y, Shinozaki T, Koibuchi H et al (2004) Primary peripheral T-cell lymphoma in subcutaneous tissue: sonographic findings. J Clin Ultrasound 32: 361–364

Galarza M, Sosa FP (2003) Pure subcutaneous seeding from medulloblastoma. Pediatr Neurol 29: 245–249

Gerster JC, Landry M, Dufresne L et al (2002) Imaging of tophaceous gout: computed tomography provides specific images compared with magnetic resonance imaging and ultrasonography. Ann Rheum Dis 61: 52–54

Giovagnorio F (1997) Sonography of cutaneous non-Hodgkin's lymphomas. Clin Radiol 52: 301–303

Giovagnorio F, Andreoli C, DeCicco ML (1999) Color Doppler sonography of focal lesions of the skin and subcutaneous tissue. J Ultrasound Med 18: 89–93

Giovagnorio F, Valentini C, Paonessa A (2003) High-resolution and color Doppler sonography in the evaluation of skin metastases. J Ultrasound Med 22: 1017–1022

Gomez EC, Berman B, Miller DL (1982) Ultrasonic assessment of cutaneous atrophy caused by intradermal corticosteroids. J Dermatol Surg Oncol 8: 1071–1074

Grechenig W, Peicha G, Clement HG et al (1999) Ultrasonographic localization of a displaced screw in the carpal canal. A case report. Acta Radiol 40: 625–627

Horton LK, Jacobson JA, Powell A et al (2001) Sonography and radiography of soft-tissue foreign bodies. AJR Am J Roentgenol 176: 1155–1159

Hwang JY, Lee SW, Lee SM (2005) The common ultrasonographic features of pilomatricoma. J Ultrasound Med 24: 1397–1402

Inampudi P, Jacobson JA, Fessell DP et al (2004) Soft-tissue lipomas: accuracy of sonography in diagnosis with pathologic correlation. Radiology 233: 763–767

Jacobson JA (2005) Musculoskeletal ultrasound and MRI: which do I choose? Semin Musculoskelet Radiol 9:135–149

Kohler R, Kritikos N, Poletti PA et al (2005) Sonographic detection of a subcutaneous twisted expander injection port. J Ultrasound Med 24: 1441–1444

Lee HS, Joo KB, Song HT et al (2001) Relationship between sonographic and pathologic findings in epidermal inclusion cysts. J Clin Ultrasound 29: 374–383

Lee HJ, Im JG, Goo JM et al (2003) Peripheral T-cell lymphoma: spectrum of imaging findings with clinical and pathologic features. RadioGraphics 23: 7–28

Lin JJ, Lin F (1974) Two entities in angiolipoma. A study of 459 cases of lipomas with review of literature on infiltrating angiolipoma. Cancer 34: 720–727

Loyer EM, DuBrow RA, David CL et al (1996) Imaging of superficial soft-tissue infections: sonographic findings in cases of cellulitis and abscess. AJR Am J Roentgenol 166: 149–152

Lyon M, Brannam L, Johnson D et al (2004) Detection of soft tissue foreign bodies in the presence of soft tissue gas. J Ultrasound Med 23: 677–681

Malherbe A, Chemantais J (1880) Note sur l'épithélioma calcifie des glandes sebacées. Prog Med 8: 826–837

Maxwell AJ, Mamtora H (1990) Sonographic appearance of epidermoid cyst of the testis. J Clin Ultrasound 18: 188–190

McGrath MH, Fleisher A (1989) The subcutaneous rheumatoid nodule (1989) Hand Clin 2: 127–135

Mellado JM, Pérez del Palomar L, Diaz L et al (2004) Long standing Morel-Lavallée lesions of the trochanteric region and proximal thigh: MRI features in five patients. AJR Am J Roentgenol 182: 1289–1294

Merki-Feld GS, Brekenfeld C, Migge B, et al (2001) Nonpalpable ultrasonographically not detectable Implanon rods can be localized by magnetic resonance imaging. Contraception 63: 325–328

Morel-Lavallée M (1863) Décollements traumatiques de la peau et des couches sous-jacentes. Arch Gen Med 1: 20–38; 172–200; 300–332

Murphey MD, Carroll JF, Flemming DJ et al (2004) Benign musculoskeletal lipomatous lesions. RadioGraphics 24: 1433–1466

Nalbant S, Corominas H, Hsu B et al (2003) Ultrasonography for assessment of subcutaneous nodules. J Rheumatol 30:1191–1195

Nazarian LN, Alexander AA, Rawool NM et al (1996) Malignant melanoma: impact of superficial US on management. Radiology 199: 273–277

Nazarian LN, Alexander AA, Kurtz AB et al (1998) Superficial melanoma metastases: appearances on gray-scale and color Doppler sonography. AJR Am J Roentgenol 170: 459–463

Nessi R, Betti R, Bencini PL et al (1990) Ultrasonography of nodular and infiltrative lesions of the skin and subcutaneous tissues. J Clin Ultrasound 18: 103–109

Neumann CG (1957). The expansion of an area of skin by progressive distension of a subcutaneous balloon: use of the method for securing skin for subtotal reconstruction of the ear. Plast Reconstr Surg 19: 124–130

Paltiel HJ, Burrow PE, Kozakewich HPW et al (2000) Soft-tissue vascular anomalies: utilities of US for diagnosis. Radiology 214: 747–754

Parra JA, Fernández MA, Encinas B et al (1997) Morel-Lavallée effusions in the thigh. Skeletal Radiol 26: 239–241

Peterson JJ, Bancroft LW, Kransdorf MJ (2002) Wooden foreign bodies: imaging appearance. AJR Am J Roentgenol 178: 557–562

Piessens SG, Palmer DC, Sampson AJ (2005) Ultrasound localization of non-palpable implanon. Aust N Z J Obstet Gynaecol 45:112–116

Rettenbacher T, Macheiner P, Hollerweger A et al (2001) Suture granulomas: sonography enables a correct preoperative diagnosis. Ultrasound Med Biol 27: 343–350

Robben SGF (2004) Ultrasonography of musculoskeletal infections in children. Eur Radiol 14: L65–L67

Roberts CC, Liu PT, Colby TV (2003) Encapsulated versus nonencapsulated superficial fatty masses: a proposed MR imaging classification. AJR Am J Roentgenol 180: 1419–1422

Scheja A, Akesson A (1997) Comparison of high frequency (20 MHz) ultrasound and palpation for the assessment of skin involvement in systemic sclerosis (scleroderma). Clin Exp Rheumatol 15: 283–288

Schmid-Wendtner MH, Burgdorf W (2005) Ultrasound scanning in dermatology. Arch Dermatol 141: 217–224

Shiels WE, Babcock DS, Wilson JL et al (1990) Localization and guided removal of soft-tissue foreign bodies with sonography. AJR Am J Roentgenol 155: 1277–1281

Soudack M, Nachtigal A, Gaitini D (2003) Clinically unsuspected foreign bodies: the importance of sonography. J Ultrasound Med 22: 1381–1385

Struk DW, Munk PL, Lee MJ et al (2001) Imaging of soft-tissue infections. Radiol Clin North Am 39: 277–303

Sy ANL, Lam TPW, Khoo US (2005) Subcutaneous panniculitislike T-cell lymphoma appearing as a breast mass: a difficult and challenging case appearing at an unusual site. J Ultrasound Med 24: 1453–1460

Thomas RH, Holt MD, James SH et al (2001) "Fat fracture": a physical sign mimicking tendon rupture. J Bone Joint Surg Br 83: 204–205

Tiliakos N, Morales AR, Wilson CH Jr (1982) Use of ultrasound in identifying tophaceous versus rheumatoid nodules. Arthritis Rheum 25: 478–479

Trop I, Dubois J, Guibaud L et al (1999) Soft-tissue venous malformations in pediatric and young adult patients; diagnosis with Doppler US. Radiology 212: 841–845

Tsai TS, Evans HA, Donnelly LF et al (1997) Fat necrosis after trauma: a benign cause of palpable lumps in children. AJR Am J Roentgenol 169: 1623–1626

Uglesic V, Knezevic P, Milic M et al (2004) Madelung syndrome (benign lipomatosis): clinical course and treatment. Scand J Plast Reconstr Surg Hand Surg 38: 240–243

Vincent LM, Parker LA, Mittelstaedt CA (1985) Sonographic appearance of an epidermal inclusion cyst. J Ultrasound Med 4: 609–611

Wilson DJ (2004) Soft-tissue and joint infection. Eur Radiol 14(Suppl 3): 64–71

White JW (1985) Evaluating cancer metastatic to the skin. Geriatrics 40: 67–72

Wortham NC, Tomlinson IP (2005). Dercum's disease. Skinmed 4: 157–162

Yen ZS, Wang HP, Ma HM et al (2002) Ultrasonographic screening of clinically-suspected necrotizing fasciitis. Acad Emerg Med 9: 1448–1451